Article

Current Biology

Sensorimotor adaptation to destabilizing dynamics in weakly electric fish

Graphical abstract

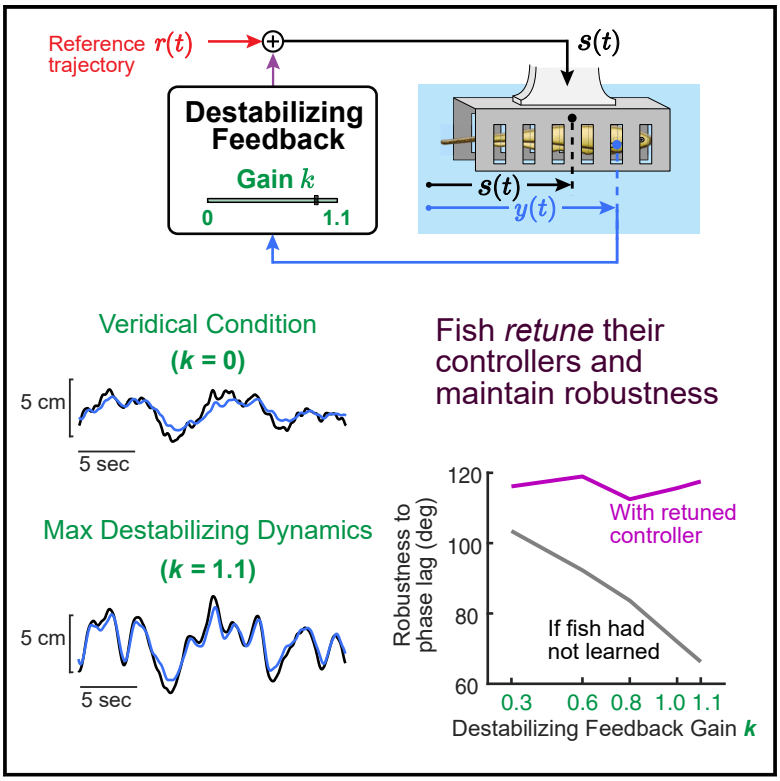

Highlights

- Fish retune their controller dynamics in response to destabilizing feedback
- Fish temporarily retain their learned controller, exhibiting a clear aftereffect
- Retuned controller improves fish tracking performance
- Retuned controller improves robustness to disturbances and uncertain phase lags

Authors

Yu Yang, Dominic G. Yared, Eric S. Fortune, Noah J. Cowan

Correspondence

yyang138@jhu.edu (Y.Y.), ncowan@jhu.edu (N.J.C.)

In brief

Using a control-theoretic framework, Yang et al. discover that electric fish learn to retune their controllers to compensate for destabilizing dynamics and retain their learned controllers, showing a clear aftereffect. Such retuning improves tracking performance, robustness to low-frequency disturbances, and measures of stability.

Yang et al., 2024, Current Biology *34*, 2118–2131
May 20, 2024
https://doi.org/10.1016/j.cub.2024.04.019

CellPress

CellPress

Current Biology

Article

Sensorimotor adaptation to destabilizing dynamics in weakly electric fish

Yu Yang,[1,2,*] Dominic G. Yared,[2] Eric S. Fortune,[3] and Noah J. Cowan[1,2,4,*]
[1]Department of Mechanical Engineering, Johns Hopkins University, 3400 N. Charles Street, Baltimore, MD 21218, USA
[2]Laboratory for Computational Sensing and Robotics, Johns Hopkins University, 3400 N. Charles Street, Baltimore, MD 21218, USA
[3]Federated Department of Biological Sciences, New Jersey Institute of Technology, 323 Dr. Martin Luther King Jr. Boulevard, Newark, NJ 07102, USA
[4]Lead contact
*Correspondence: yyang138@jhu.edu (Y.Y.), ncowan@jhu.edu (N.J.C.)
https://doi.org/10.1016/j.cub.2024.04.019

SUMMARY

Humans and other animals can readily learn to compensate for changes in the dynamics of movement. Such changes can result from an injury or changes in the weight of carried objects. These changes in dynamics can lead not only to reduced performance but also to dramatic instabilities. We evaluated the impacts of compensatory changes in control policies in relation to stability and robustness in *Eigenmannia virescens*, a species of weakly electric fish. We discovered that these fish retune their sensorimotor control system in response to experimentally generated destabilizing dynamics. Specifically, we used an augmented reality system to manipulate sensory feedback during an image stabilization task in which a fish maintained its position within a refuge. The augmented reality system measured the fish's movements in real time. These movements were passed through a high-pass filter and multiplied by a gain factor before being fed back to the refuge motion. We adjusted the gain factor to gradually destabilize the fish's sensorimotor loop. The fish retuned their sensorimotor control system to compensate for the experimentally induced destabilizing dynamics. This retuning was partially maintained when the augmented reality feedback was abruptly removed. The compensatory changes in sensorimotor control improved tracking performance as well as control-theoretic measures of robustness, including reduced sensitivity to disturbances and improved phase margins.

INTRODUCTION

Animals routinely alter their behavior in response to novel sensorimotor dynamics. For example, insects can retune their neural control systems and maintain function after limb amputation,[1–4] antenna trimming,[5,6] and wing damage.[7–9] Humans and other animals can routinely learn new motor behaviors and retune existing ones through practice.[10] The mechanisms and strategies for such motor learning are currently being revealed,[10] including at the circuit level.[11–15]

As an animal retunes its sensorimotor control system in response to changes to system dynamics, it must maintain *stability*. Although there are many definitions of stability,[16] here we refer to a system's convergence to a desired goal point or trajectory from a local neighborhood of possible initial system states. A complementary question is, how does the retuned sensorimotor loop affect system *robustness*, i.e., how well does the system achieve stability and convergence despite external perturbations[17] or changes in internal parameters?[18]

To address these questions, we studied a well-suited model system, refuge tracking in the weakly electric glass knifefish *Eigenmannia virescens*. *Eigenmannia* has been likened to an "aquatic hummingbird,"[19] smoothly hovering in place or making agile movements to track a moving refuge.[20] These fish swim back and forth to sense their position,[21–24] while tracking the movements of a refuge.[20,25,26] Fore-aft swimming movements are produced in *Eigenmannia* by rostro-caudal adjustments of the position of the nodal point, where counter-propagating waves of its ventral ribbon fin meet.[18,27]

Here, we examined sensorimotor adaptation to experimentally induced changes in sensorimotor dynamics in this refuge tracking behavior using an augmented reafferent feedback loop (Figure 1A). Normally (in the veridical case), fore-aft swimming movements generate one-to-one motion of the refuge across its visual and electrosensory receptors, but in the opposite direction (corresponding to the negative sign in the veridical reafferent feedback signal, Figure 1B). Our refuge system augmented this reafferent feedback by digitizing the fish position in real time from video camera images, passing the digitized fish position through a high-pass filter and feeding the resulting signal back to the refuge position (Figure 1B, augmented reafferent loop).

A key innovation of the experimental manipulation was to high-pass filter the augmented reafferent feedback to gracefully destabilize the closed-loop system. When the fish generated low-frequency movements (i.e., below the cut-off frequency of the high-pass filter), reafferent feedback was approximately veridical—little experimental change in feedback was made. In contrast, when the fish rapidly changed direction (i.e., high-frequency, back-and-forth movements), such movements were

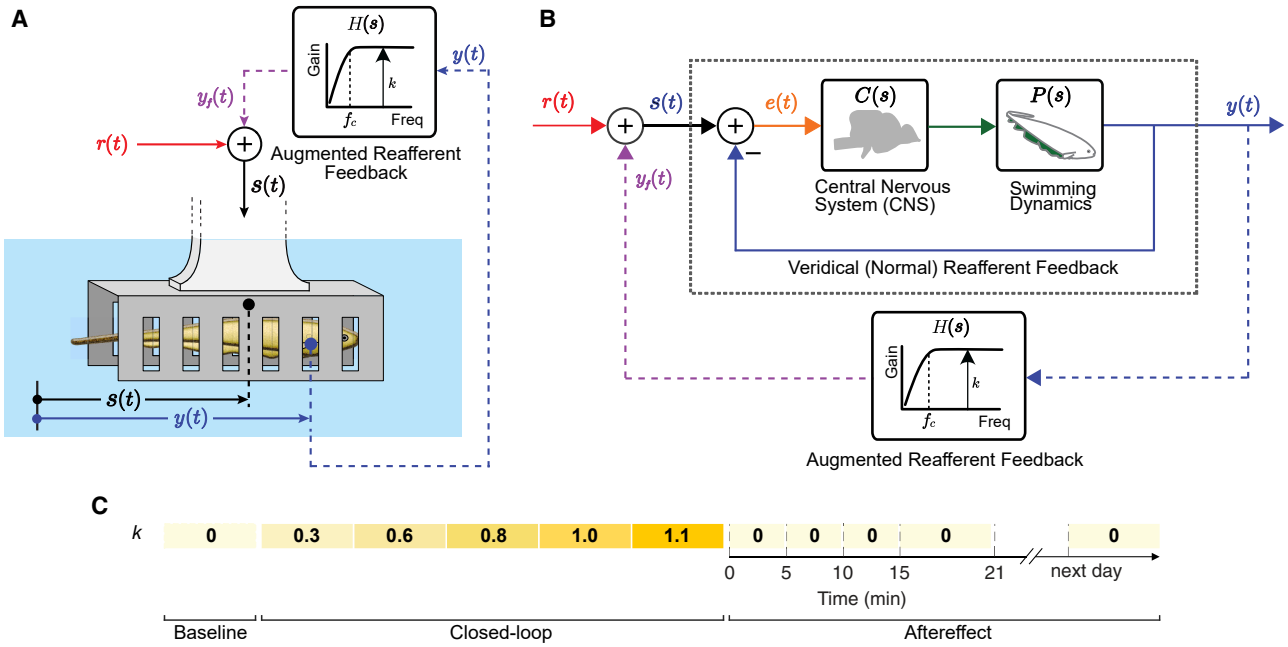

Figure 1. Experimental protocol and stimulus design

(A) Schematic of the augmented, destabilizing feedback system. The longitudinal fish position, $y(t)$, was measured in real time using a custom video tracking system and processed through a high-pass filter, $H(s)$ with gain k and cut-off frequency $f_c = 0.16$ Hz, where s is the complex frequency-domain parameter. The high-pass-filtered position, $y_f(t)$, was then added to a pseudo-random (sum-of-sines) reference signal $r(t)$, and fed to the refuge, i.e., $s(t) = y_f(t) + r(t)$, creating an augmented reafferent loop.

(B) Block diagram of the closed-loop system depicted in (A). The augmented, high-pass-filtered feedback loop is closed around the fish sensorimotor system (black dotted box). The fish senses the difference between the longitudinal refuge position $s(t)$, and its own reafferent feedback $y(t)$. This difference $e(t)$ ("sensory slip"[21]) is then processed by the nervous system, $C(s)$, and swimming dynamics, $P(s)$.

(C) Protocol: experiments started from an experimental open-loop baseline period ($k = 0$), followed by a closed-loop period in which we incrementally increased the gain k of the high-pass-filtered augmented feedback from 0.3 to 1.1 over a period of about 33 min. Finally, we extinguished the augmented feedback ($k = 0$) to test for aftereffects. The sensorimotor controller was tested at five time intervals during the aftereffect period: 0 to 5, 5 to 10, 10 to 15, and 15 to 21 min, and the next day.

amplified and fed back to the refuge. Importantly, the gain of this high-pass-filtered feedback was gradually increased (Figure 1C), incrementally driving the closed-loop control system toward instability, providing ample opportunity for the fish to learn to compensate for the manipulation while successfully performing the refuge tracking behavior. This manipulation was "graceful" in comparison with standard paradigms that use abrupt and categorical (broad-band) gain reversals to destabilize closed-loop dynamics.[28–32]

Previous efforts to destabilize a feedback loop typically involve inverting the feedback gain[28,29] (e.g., a mirror reversal in visuomotor tasks). Inversion of feedback gain instantaneously and abruptly destabilizes system dynamics. This destabilization is not graceful—the animal's performance is dramatically degraded by the experimental change in feedback.[28] Animals can, over extended periods of time, learn to compensate for these changes in feedback: humans can take many days to learn to compensate for mirror-reversal manipulations.[30] The approach we used here, increasing the gain of the high-pass filter, slowly leads to a gain reversal for high-frequency movements, while leaving low-frequency movements veridical. In this way, the animal can continuously perform the task while it retunes its sensorimotor control system in response to increasingly strong destabilizing dynamics. Unlike classic mirror reversals, we found that this retuning under high-pass-filtered feedback can occur within a single experimental session of about 33 min in duration.

As we increased the gain of the high-pass filter in the augmented reafferent feedback loop, we simultaneously injected pseudo-random motions of the refuge, allowing us to determine the sensorimotor dynamics of each fish using a technique known as system identification (i.e., stimulus-response modeling).[19,33] We then removed the augmented reafferent feedback (returning to the veridical condition) to assess any retention in the sensorimotor controller, using the aftereffect as an indicator of learning. Finally, we performed control-theoretic analyses as a normative framework to interpret the benefits of the learned controller. Using this framework, we discovered that the nervous system maintained robustness to both low-frequency disturbances and uncertain phase lags.

RESULTS

We designed an augmented reafferent feedback loop to alter the closed-loop dynamics that fish experienced during refuge tracking (Figures 1A and 1B). Specifically, we fed fish position back through a high-pass filter in real time and added it to a predefined pseudo-random sum-of-sines input (Figure S1A).[26,30] To

drive the closed-loop system toward instability, we incrementally increased the augmented feedback gain, *k*, of the high-pass-filtered feedback (Figure 1C). The experiments started from open loop, the baseline veridical condition. This was followed by a closed-loop period in which the gain of the high-pass-filtered feedback was gradually increased. This feedback was designed based on preliminary analysis[34] to destabilize the behavioral system and elicit learning. Finally, we removed the augmented feedback to assess aftereffects.

Fish retuned their controller dynamics in response to destabilizing feedback

We observed that the increase in the augmented feedback gain *k* caused a commensurate increase in the refuge and fish velocities (Figures 2A–2C). To understand how the augmented feedback changed the fish's tracking response, we performed frequency-domain system identification from time-domain position data (sampled data shown in Figures S1B–S1D) of seven individual fish. These experiments allowed us to estimate the empirical frequency response functions (FRFs) of individual fish. The empirical frequency response estimates, which compare the Fourier spectra of the fish movement with that of the refuge, are completely data driven (see STAR Methods). The FRFs comprised the entire sensorimotor transform, including the fish's veridical reafferent feedback (see black dotted box in Figure 1B), but excluded the augmented feedback. Using this method, we assessed how changes to the augmented feedback (via the gain *k*) led to changes in the fish's control system (as measured through its frequency response).

We found that fish systematically retuned their controllers under augmented feedback. Fish increased sensorimotor gain, especially at higher frequencies (above 1 Hz) and added phase leads at intermediate frequencies (around 0.65 Hz) in response to the increasing augmented feedback gain *k* (Figure 2D). This trend of increased gain and phase at the frequencies 1.15 Hz (gain) and 0.65 Hz (phase) was observed in each of seven fish (Figures 2E and 2F). These frequencies were selected post hoc based on visual inspection of the frequency responses.

Fish temporarily retained their learned controller, exhibiting a clear aftereffect

We examined the performance of fish immediately after the closed-loop feedback was abruptly removed: the presence of aftereffects may suggest the involvement of a plasticity-based mechanism such as cerebellar learning.[30,35,36]

If the control system of a fish was retuned by tracking under augmented feedback, evidence of that retuning should emerge when it is removed. In other words, we expected to measure an aftereffect—a residual change in behavioral performance compared with baseline performance—immediately after the augmented feedback was extinguished. To assess aftereffects in the fish's controller, we averaged the frequency responses in blocks of three or five trials during the aftereffect period (see Figure 1C) and compared the result with the baseline frequency response. Figures 3A and S2A show the mean fish frequency response gain and phase during the aftereffect period, as well as the baseline period, from a representative fish. Note that in both baseline and aftereffect periods, the fish was under veridical feedback with no augmented high-pass filter in the feedback loop.

Immediately after the augmented feedback was removed, both the gain and phase of this fish remained elevated (Figures 3A and S2A), revealing that the retuned controller persisted. This is similar to the persistent retuning of reach direction in visuomotor learning experiments in humans.[10] The sensorimotor gain washed out over a period of about 10 min, as indicated by the frequency response gain returning to baseline (Figure 3A). The elevated phase appeared to persist for longer, returning to baseline on the next day (Figure S2A).

This result generalized across fish. We compared mean fish frequency response gain and phase at 1.15 and 0.65 Hz during the aftereffect periods for six fish. As before, these frequencies were selected post hoc because they showed clear changes in gain and phase during retuning to augmented feedback (see Figures 2D–2F). As shown in Figure 3B, fish partially retained their gain at 1.15 Hz after the augmented reafferent feedback was extinguished: in the first 5 min in the aftereffect period, the gain was significantly greater than baseline ($p < 0.01$, paired-sample t test in dB; Table S2). Similarly, as seen in Figure S2B, the phase at 0.65 Hz was also partially retained after learning: the phase at 0.65 Hz during the first 5 min of the aftereffect period was significantly greater than baseline ($p < 0.05$, paired-sample t test; Table S3).

Interestingly, we observed that gain and phase washed out over different time courses. The fish gain at 1.15 Hz washed out relatively quickly. The gain after the augmented feedback was extinguished was significantly lower in the second 5-min period than in the first 5-min period ($p < 0.05$, two-sided sign test; Figure 3B). Moreover, the gain was statistically indistinguishable from baseline for all subsequent test periods ($p > 0.1$, paired-sample t test in dB; Figure 3B; Table S2). In contrast, the phase at 0.65 Hz washed out more slowly, as fish frequency response phases were significantly greater than baseline phase for multiple consecutive 5-min internals ($p < 0.05$, paired-sample t test; Table S3), returning to baseline by the next day ($p > 0.2$, paired-sample t test; Figure S2B; Table S3).

The significant aftereffect quantified using frequency response methods was also apparent in the time-domain data. Figure 3C shows the aftereffect in the time domain, comparing the velocity tracking error $\dot{e}(t)$, i.e., $\dot{e}(t) = \dot{s}(t) - \dot{y}(t)$, in the baseline period with the first 8 s of the aftereffect period from an example fish. The velocity tracking error $\dot{e}(t)$ in the first 8 s of the aftereffect period was markedly different from mean ± standard deviation of baseline. To better highlight the behavioral differences, we filtered velocity tracking errors in baseline and the first 8 s of aftereffect with a second-order bandpass Butterworth zero-phase distortion filter. The lower and higher cut-off frequencies were chosen to be 0.7 and 1.3 Hz, as we found that fish showed most noticeable changes of their frequency responses in that frequency band in Figure 2D. The time-domain data in this frequency band highlights the higher amplitudes and a clear phase lead (earlier peaks and troughs) of the velocity error for the retuned and partially retained sensorimotor system compared with the (untuned) baseline performance (Figure 3D).

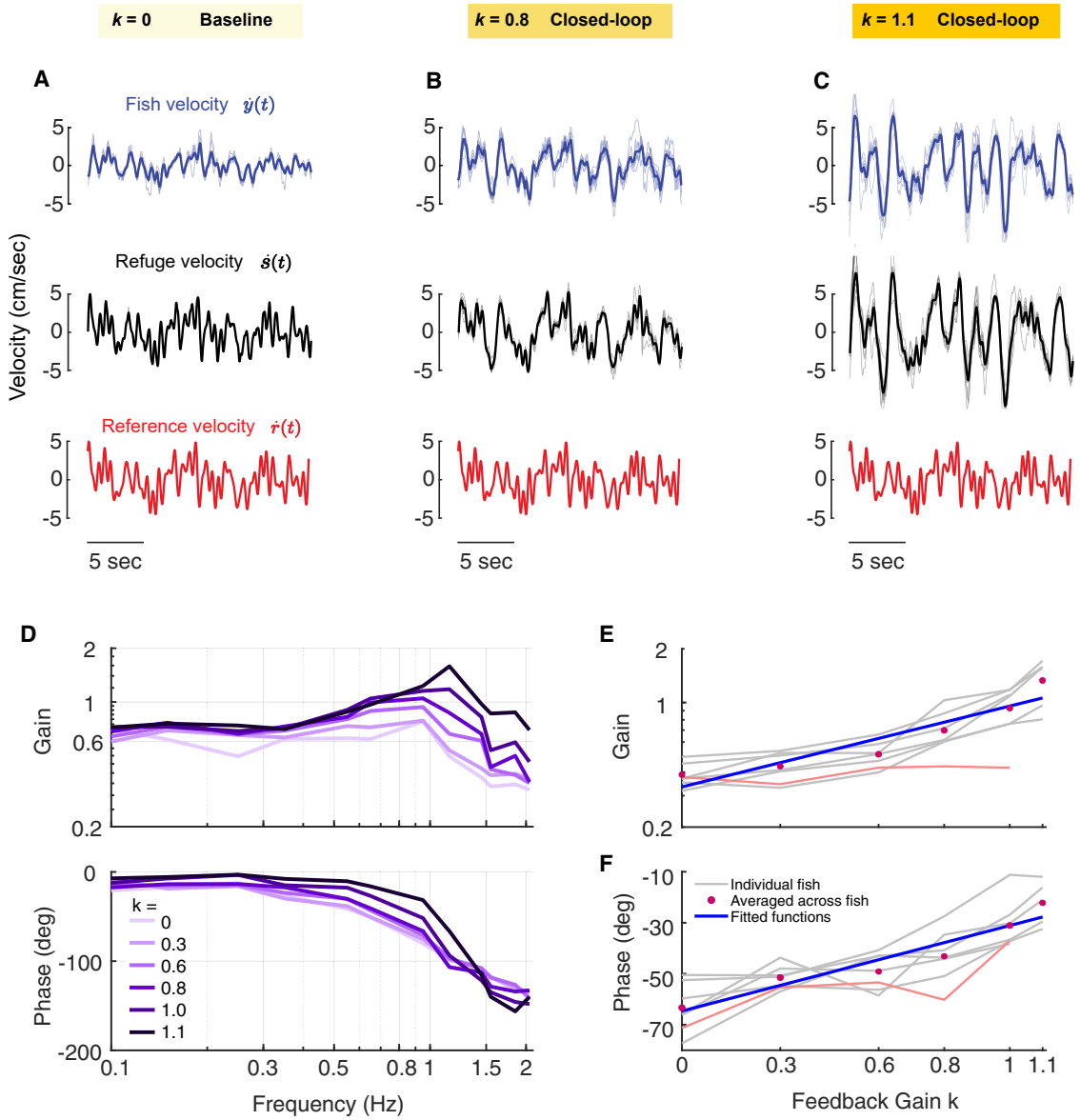

Figure 2. Fish retuned their controller dynamics in response to destabilizing feedback

(A–C) From top row to bottom row: fish velocity $\dot{y}(t)$, refuge velocity $\dot{s}(t)$, and reference velocity $\dot{r}(t)$ in time domain in (A) veridical baseline, (B) closed-loop $k = 0.8$, and (C) closed-loop $k = 1.1$. The thick lines are the mean and thin lines are individual trials. We observed that, as the gain in augmented high-pass feedback increased, both fish and refuge had higher velocity magnitude (see Figure S1 for position data).

(D) Frequency response of a representative fish. As the feedback gain was increased, the gain of the frequency response function also increased (especially around 1.15 Hz) and the phase lag decreased (most strikingly at frequencies around 0.65 Hz).

(E and F) (E) Gain of fish frequency response functions at 1.15 Hz and (F) phase at 0.65 Hz as a function of feedback gain k (seven fish for most points, except for $k = 1.1$ where two fish were excluded due to poor data quality). Linear functions (blue lines) were fitted to the mean gains (pink dots) in logarithmic scale at 1.15 Hz, and mean phases (pink dots) in linear scale at 0.65 Hz across all individual fish (gray curve). Six out of seven fish exhibited significant ($p < 0.05$) positive correlations between high-pass gain k and common logarithm ($\log_{10}$) of gain at 1.15 Hz ($\rho(3) = 0.93$ for one fish, $\rho(4) > 0.91$ for the other five fish) or phase at 0.65 Hz ($\rho(3) = 0.92$ for one fish, $\rho(4) > 0.86$ for the other five fish); one fish (red line) exhibited positive, but non-significant correlations for both gain ($\rho(3) = 0.76$, $p > 0.1$) and phase ($\rho(3) = 0.80$, $p > 0.1$). Statistical details are in Table S1.

See also Figure S1 and Table S1.

Advantage (1): Retuned controller improved tracking performance

Fish retuned their controllers under the augmented, destabilizing feedback. To understand the possible benefits of this adaptive control process, we examined how the retuned controllers impacted fish tracking performance. We computed the fish's velocity tracking error $\dot{e}(t)$ in each experiment by taking the backward differences of fish position data. We used the baseline empirical FRF for each fish to simulate that fish's velocity tracking error in each augmented feedback period. This

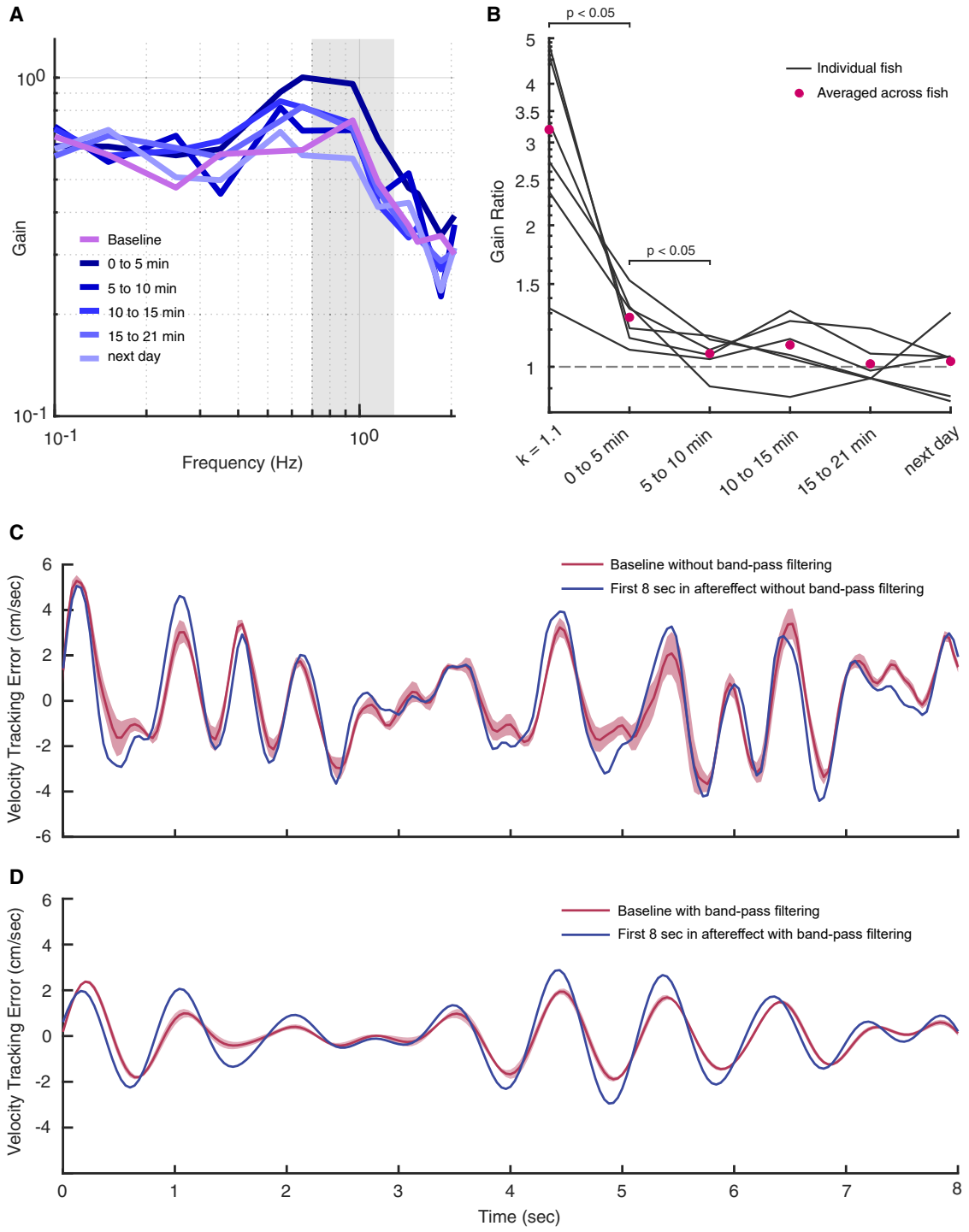

Figure 3. Fish temporarily retained learned controller during an aftereffect period

(A) Mean frequency response gain from an example fish for the baseline (pre-learning) and five time periods after the augmented feedback was removed (aftereffect). The gain of the frequency response remained elevated immediately after the augmented feedback was removed (0 to 5 min), washing out within about 10 min. Changes in the phase of the frequency response during the aftereffect period are in Figure S2 and statistical details related to phase are in Table S3.

(B) *Gain ratio* for six fish (black) and their mean (pink dots). Gain ratio was calculated as the mean fish frequency response gain divided by baseline mean frequency response gain at 1.15 Hz. Time windows include the augmented feedback $k = 1.1$ period, four non-overlapping windows after the augmented feedback was removed, and the next day. The gain in the first 5 min after the removal of the augmented feedback was significantly lower than that in $k = 1.1$ ($p < 0.05$, two-sided sign test) but remained higher than baseline ($p < 0.01$, paired-sample t test in dB; Table S2), indicating retention of the learned controller. The gain in the subsequent periods was not significantly higher than baseline ($p > 0.1$, paired-sample t test in dB; Table S2).

(legend continued on next page)

simulation used phasor analysis based on the raw FRF (without any model fitting) at each stimulus frequency to predict what would have happened in the theoretical case that the fish *had not* retuned its controller under destabilizing augmented feedback (Figure 4A); see STAR Methods and Roth et al.[37]

To compare the observed and simulated tracking performances, we computed the root-mean-square (RMS) velocity tracking error: lower RMS velocity tracking errors correspond to better tracking performance. We compared observed (retuned) RMS velocity tracking error with the corresponding simulated (no retuning) error. Across all seven fish and nearly all gains (29 of 33), the observed RMS velocity tracking error for the retuned controller was significantly less than that of the simulations with no retuning ($p < 0.001$, two-tailed Mann-Whitney-Wilcoxon test; Figure 4B).

To corroborate the time-domain error velocity analysis, we examined the normalized error $|E(j\omega)/R(j\omega)|$ in the frequency domain for all five feedback gains (Figure 4C). Similar to the time-domain analysis, we used the individual baseline controller for each fish to predict what would have happened were the fish *not* to have retuned its controller when we introduced the destabilizing augmented feedback. We integrated (area under the curve in the frequency domain) the normalized observed and predicted tracking error for all seven fish. We found that across all fish and 32 of 33 gains, the observed frequency-domain error for the retuned controller was significantly less than that predicted when assuming no retuning ($p < 0.001$, two-tailed Mann-Whitney-Wilcoxon test; Figure 4D). In sum, the retuned controllers decreased both the RMS velocity tracking error and the normalized error compared with the prediction assuming no retuning.

Advantage (2): Retuned controller reduced sensitivity to disturbance

The *sensitivity function* $S(j\omega)$ (see STAR Methods) reflects how well a feedback system suppresses disturbances at each radian frequency ω.[38] Disturbances comprise perturbations to the motor plant, such as neuromuscular noise[39] and turbulence.[40] At frequencies ω for which $|S(j\omega)| < 1$ (indicating *robustness*), a system *attenuates* disturbances. Conversely, a system *amplifies* disturbances when $|S(j\omega)| > 1$ (indicating *fragility*).[38,41] Critically, for many systems, there is a trade-off between robustness and fragility because of a general result known as the "waterbed effect"[38]: the integral of the natural log of the sensitivity function magnitude—i.e., the *Bode sensitivity integral*—is 0:

$$\int_0^\infty \ln(|S(j\omega)|)d\omega = 0. \qquad \text{(Equation 1)}$$

This integral constraint implies that suppressing disturbances ($\ln|S| < 0$, indicating *robustness*) at some frequencies requires amplifying disturbances ($\ln|S| > 0$, indicating *fragility*) at other frequencies. This result depends on certain technical requirements of the system dynamics[38] that we believe to be satisfied (see STAR Methods for details).

We computed the predicted sensitivity function for each augmented feedback gain, k, based on each fish's baseline controller (estimated in the veridical condition—no augmented feedback). These calculations were based on the empirical frequency response data without analytical modeling; see STAR Methods for details. This predicted sensitivity was compared with the sensitivity function that each fish achieved when the augmented feedback was applied. If the fish had not changed their controller, then the predicted and observed sensitivity functions would have been identical.

For both the predicted and observed sensitivity functions, we approximated the Bode sensitivity integral over the experimental bandwidth of 0.1 – 2.05 Hz (0.63 – 12.9 rad/s) using trapezoidal integration (with respect to ω rad/s). Figure 5A shows the natural logarithm of sensitivity function magnitude (predicted and observed) at $k = 1.1$ from one representative fish over this bandwidth. As the augmented feedback gain k was increased, the sensitivity integral became increasingly negative compared with the predicted integral ($p < 0.05$ for $k = 0.3$, $p < 0.01$ for each $k > 0.3$, paired-sample t test) (Figure 5B; Table S4). This indicates that the retuned fish controller improved the overall robustness with respect to disturbances.

We also computed "sensitivity crossover frequency" for each feedback gain for all seven fish, i.e., the frequency at which the natural logarithm of sensitivity function magnitude $\ln|S(j\omega)|$ crossed 0 for the first time. A total of 28 of 32 points are located below the identity line, showing that the retuned controller increased the sensitivity crossover frequency compared with the predicted crossover frequency across all seven fish and for nearly all gains (28 of 32) ($p \approx 0.001$, two-tailed Mann-Whitney-Wilcoxon test, Figure 5C). Thus, the retuned controller attenuated disturbances over a wider bandwidth than if it had not been retuned.

These findings indicate that the retuning of fish controllers significantly reduced sensitivity to disturbances. This enhancement became more pronounced with ever-increasing augmented feedback gains, as the difference between the observed and simulated Bode integral decreased with increased gain k ($p < 0.05$, correlation coefficient $\rho(3) = -0.94$ for the mean across seven fish in five feedback periods).

Advantage (3): Retuned controller improved PM

We examined how changes in the fish's sensorimotor controller affected closed-loop *stability robustness*, i.e., the ability of a system to maintain stability despite changes in internal system parameters. Similar to our previous analyses, we used the fish's baseline frequency response—before the destabilizing augmented feedback was introduced—to mathematically predict

(C) Comparison of velocity tracking error $\dot{e}(t) = \dot{s}(t) - \dot{y}(t)$ in baseline (pink, veridical) and first 8 s of aftereffect (blue, also veridical but after learning) from a single fish. Shaded region indicates standard deviation. During the first 8 s after the removal of the augmented reafferent feedback, the amplitude of velocity tracking error was greater than that in baseline most of the time, reflecting the temporary retention of the controller obtained during learning.
(D) Filtered velocity tracking errors in baseline and first 8 s of aftereffect from the fish in (C). The filter used was a second-order bandpass Butterworth zero-phase distortion filter (pass band: 0.7 to 1.3 Hz, gray shaded region in A). Filtering to this frequency band clearly illustrates that during the first 8 s of aftereffect, fish exhibited higher amplitude velocity tracking errors and substantial phase lead compared with baseline.
See also Figure S2 and Tables S2 and S3.

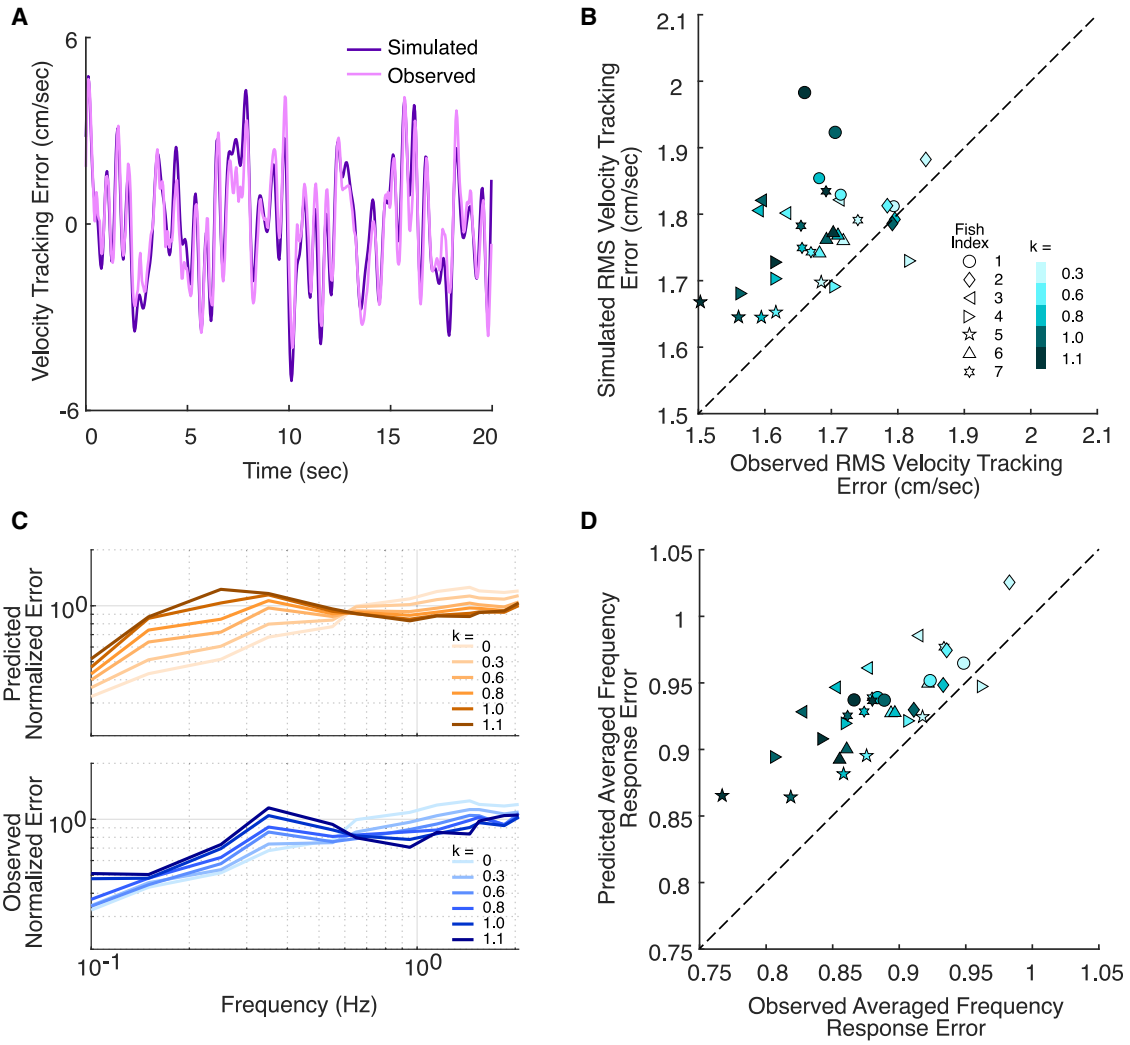

Figure 4. Retuned controller improved tracking performance

(A) Simulated velocity tracking error (prediction, purple) during the $k = 1.1$ period using the baseline controller of one fish and the observed velocity tracking error from the same fish during that period (observed, pink). The observed tracking error was generally lower in amplitude than the prediction made using the baseline controller, most notably as a result of large spikes in the predicted error.

(B) Scatterplot showing the simulated and observed root-mean-square (RMS) velocity tracking error for each feedback gain, for seven fish. A total of 29 of 33 points from all seven fish are located above the identity line, showing that the retuned controller decreased RMS velocity tracking error ($p < 0.001$, two-tailed Mann-Whitney-Wilcoxon test).

(C) The predicted normalized error $|E(j\omega)/R(j\omega)|$ was computed by assuming that the fish did not retune their baseline controller as the feedback gain was increased; $R(j\omega)$ and $E(j\omega)$ are the frequency-domain reference signal $r(t)$ and sensory slip $e(t)$, respectively. As can be seen for a representative fish (top), when the high-pass gain k increased, the predicted normalized error increased substantially below about 0.6 Hz, and decreased slightly for higher frequencies. In contrast, the observed error below about 0.6 Hz measured for the same fish (bottom) was substantially lower than the predicted error in that frequency range, as the retuned controller largely mitigated the effects of the destabilizing feedback.

(D) Scatterplot showing the predicted and observed averaged frequency response error, integrated across the frequency range of 0.1 – 2.05 Hz, for each feedback gain, for seven fish. Fish index and feedback gain color scale same as (B). A total of 32 of 33 points from across all fish are located above the identity line, showing that the retuned controller decreased normalized tracking error over predicted normalized tracking error ($p < 0.001$, two-tailed Mann-Whitney-Wilcoxon test).

closed-loop performance and compared this baseline prediction to the observed retuned control system. We observed that fish maintained or improved measures of stability robustness compared with what would be expected if the fish had not retuned their controller.

To quantify stability robustness, we used two concepts from control theory, namely the *gain margin* (GM) and *phase margin* (PM), which provide measures of how much a system can be perturbed before it becomes unstable. Under technical assumptions (see STAR Methods), the GM measures how close the gain of the loop function is to unity gain (0 dB) at the frequency where the phase of the loop function crosses -180°. Likewise, the PM measures how much the phase of the loop function is above -180° at the frequencies where the gain crosses 0 dB (see

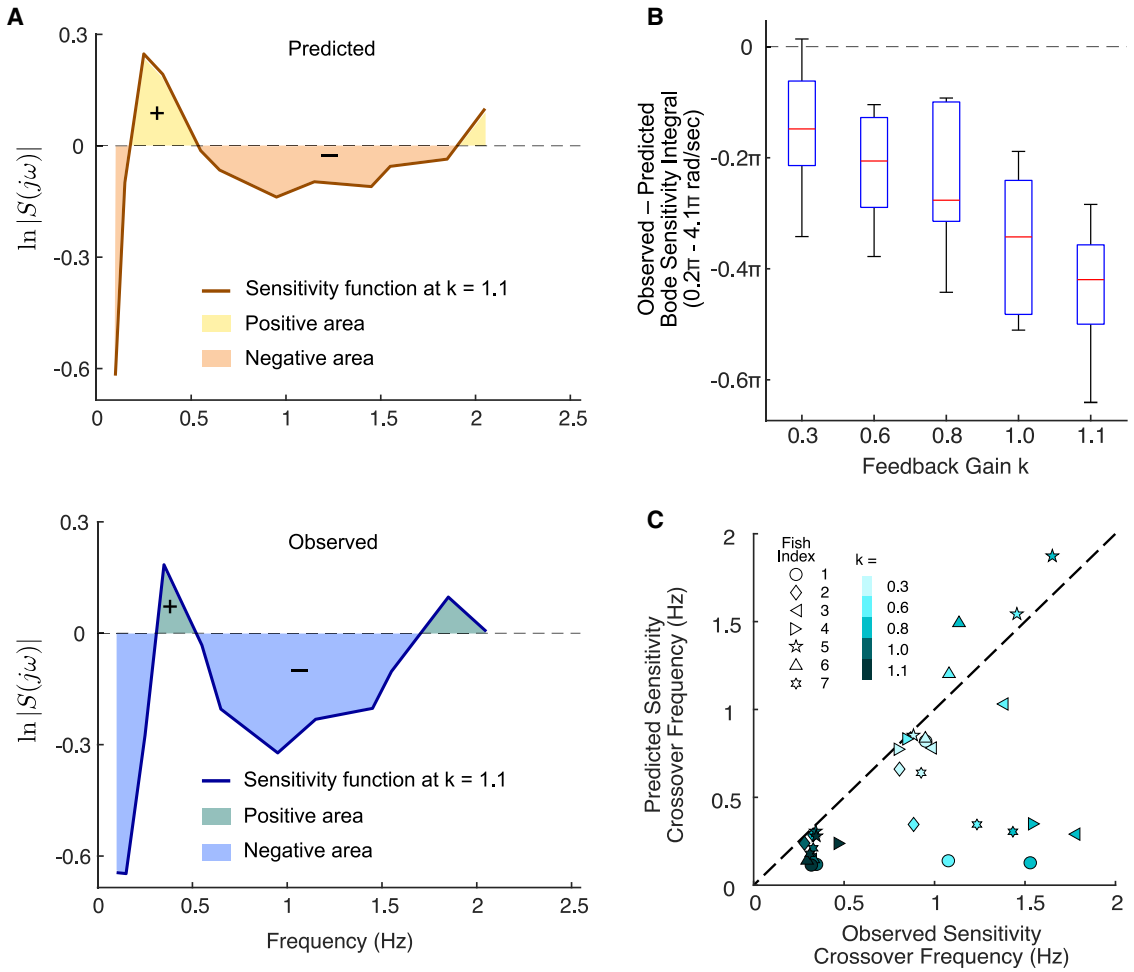

Figure 5. Tuned controller reduced sensitivity to disturbance

(A) Predicted (based on baseline controller) and observed (based on fish's retuned controller) Bode sensitivity functions for $k = 1.1$, from one representative fish. The natural logarithmic magnitude of the observed Bode sensitivity function has a larger negative region than predicted (see Figure S3 for larger frequency range).

(B) For each individual fish, and at each gain k, we computed the difference between the observed and predicted Bode sensitivity integrals over the frequency range 0.1 – 2.05 Hz (0.2π–4.1π rad/s). Box and Whisker plots of these values are shown for all seven fish for $k = 0.3 - 1.0$, five fish for $k = 1.1$. The mean value across all fish was < 0 for each gain ($p < 0.05$ for $k = 0.3$, $p < 0.01$ for the remaining gains, paired-sample t test for observed versus predicted Bode sensitivity integral). Statistical details are in Table S4.

(C) Scatterplot showing the predicted and observed sensitivity crossover frequency for each feedback gain, for seven fish. Note that here we report only the frequency at which natural logarithm of sensitivity function magnitude $\ln|S(j\omega)|$ crosses 0 for the first time. A total of 28 of 32 points are located below the identity line, showing that the retuned controller increased sensitivity crossover frequency over predicted sensitivity crossover frequency for all seven fish, and for nearly all gains (28 of 32) ($p \approx 0.001$, two-tailed Mann-Whitney-Wilcoxon test).

See also Figure S3 and Table S4.

Figure 6A). Here, the loop function $L = CP(1 - DH)$ includes the fish's own controller and plant, $C(s)$ and $P(s)$, the setup delay in the forward loop $D(s)$, as well as the augmented high-pass filter feedback, $H(s)$.

For the sensorimotor dynamics considered here, these measures of robustness are simple and intuitive: if at any frequency the loop function L reaches the -1 point, then at that frequency the sensory slip $e(t)$ experiences *positive* feedback due to the negative sign in the reafferent loop (Figure 1B), rendering the system *unstable*. Further, the -1 point has unity gain (0 dB) and -180° phase. Therefore, when L gets close to the -1 point, small changes in the sensorimotor dynamics could push the system into instability. In this way, the GM and PM are measures of stability robustness, i.e., measures of the safety margin between the observed loop function and the -1 point.

If the fish were to have maintained its baseline performance, the PM would have decreased substantially as we increased the augmented feedback gain k (Figure 6B). Note that this predicted PM demonstrates that the augmented feedback achieved the goal of destabilizing the system, i.e., driving down the PM. The difference between observed PM and predicted PM was significantly above 0° for all augmented feedback gains ($p < 0.05$, paired-sample t test; Figure 6C; Table S5). Moreover, as the augmented feedback gain k increased, the difference between observed PM and predicted PM increased ($p < 0.01$, correlation coefficient $\rho(3) = 0.97$ for

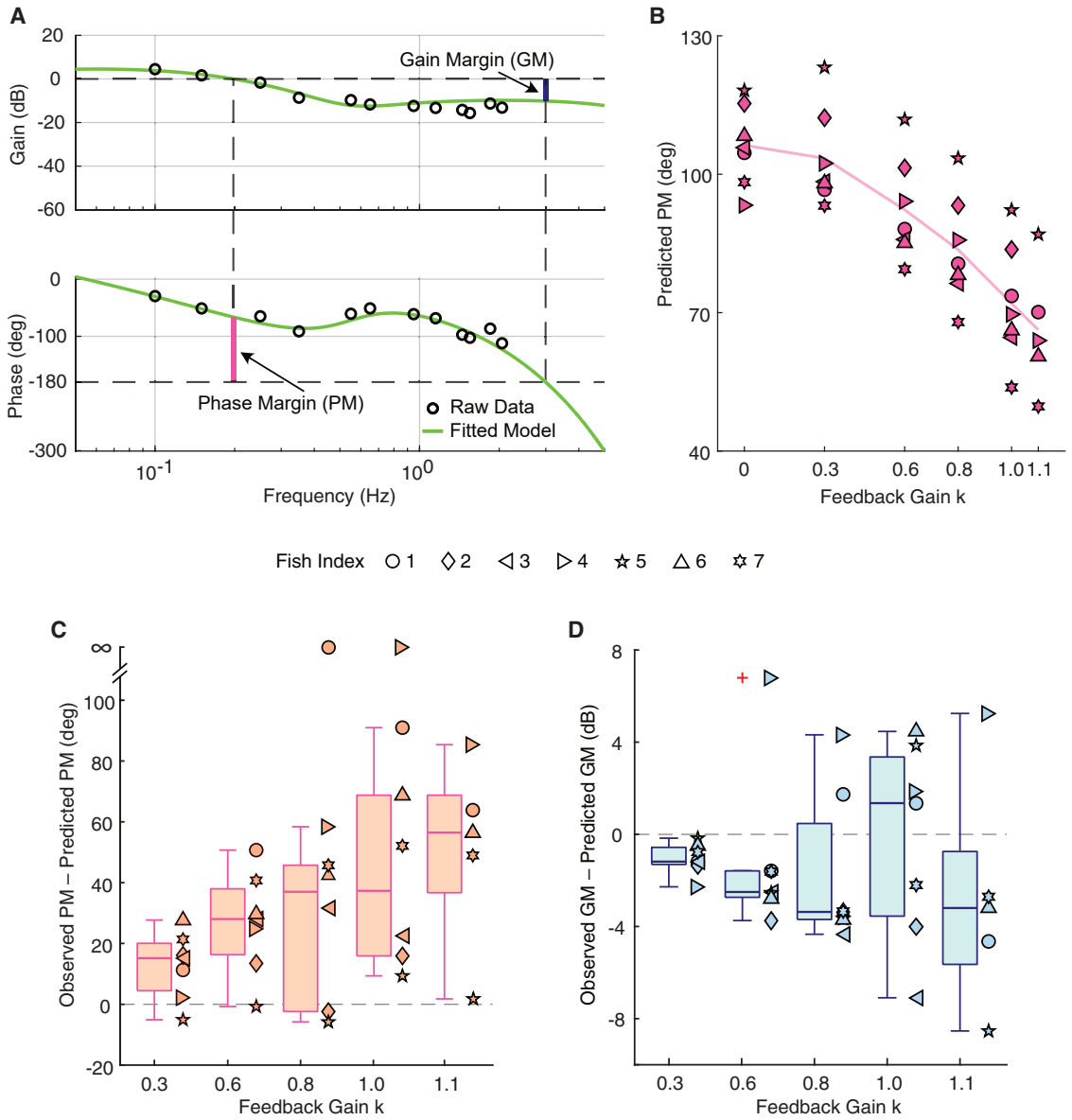

Figure 6. Tuned controller improved phase margin and maintained gain margin, measures of stability robustness

(A) Illustration of the *gain margin* (GM) and *phase margin* (PM) with raw data (black circles) and fitted model (green line) from one fish in $k = 0.8$ period. We used fitted models (see STAR Methods) when computing the GM and PM because the exact gain and phase crossover frequencies must be interpolated or extrapolated from the raw data, as shown.

(B) Predicted PM in $k = 0$ (baseline) and all five closed-loop periods from seven fish, computed from the model. As feedback gain increased, the predicted PM dropped, showing that the experimental design destabilized the closed-loop system as expected.

(C) Boxplot of the difference between observed and predicted PM as a function of feedback gain k for seven fish (computed from model). The difference is significantly greater than 0° in all feedback periods ($p < 0.05$, paired-sample t test; Table S5), indicating that the retuned controller enhanced PM. Note that two data points (fish 1, $k = 0.8$ and fish 4, $k = 1.0$) were excluded from the statistical analysis because they had infinite observed PM (loop function gain never crossed 0 dB) despite a finite predicted PM.

(D) Boxplot of the difference between observed and predicted GM as a function of feedback gain k for seven fish (computed from model); a value > 0 dB (or < 0 dB) implies that the retuned controller increased (or decreased, respectively) GM. The difference is not consistently above or below 0 dB as a function of feedback gain k (Table S6), and there is no significant correlation ($p > 0.1$) between high-pass gain k and the difference between observed and predicted GM averaged across seven fish. Therefore, the retuned controller did not significantly enhance GM.

See also Tables S5 and S6.

the mean across seven fish in five feedback periods). Notably, the improvement in PM for $k = 1.1$ was around 50°, indicating that the retuning seen in Figures 2D–2F led to a substantial improvement in PM. Note that the statistical results for PM did not include data from one fish in feedback period $k = 0.8$ and a different fish in period $k = 1.0$ because both of their

observed loop functions did not cross 0 dB. Nevertheless, these excluded data also support our finding (i.e., infinite observed PM versus finite predicted PM). In summary, fish improved their PM compared with prediction.

For the GM, as the augmented high-pass feedback gain k was increased, the mean difference between observed and predicted GM across seven fish remained near 0 dB (Figure 6D). At two gains (0.3 and 0.6), the retuned controller decreased GM when outliers were removed (before removing outliers: $p < 0.01$ for $k = 0.3$, $p > 0.2$ for remaining periods, paired-sample t test; after removing outliers: $p < 0.01$ for $k = 0.3$, $p < 0.001$ for $k = 0.6$, $p > 0.2$ for remaining periods, paired-sample t test; Table S6). There was no significant trend as a function of k ($p = 0.583$, $\rho(3) = -0.33$ before removing outliers and $p = 0.818$, $\rho(3) = -0.14$ after removing outliers).

In sum, the fish's retuned closed-loop system was robust with respect to augmented feedback, which was designed to drive the closed-loop system toward instability. These results indicate that the retuned controller maintained GM and substantially improved PM, two common measures of stability robustness.

DISCUSSION

We examined how weakly electric fish changed their refuge tracking behavior in response to an innovative experimental paradigm—the gradual introduction of destabilizing dynamics via the application of high-pass-filtered augmented feedback. The changes in behavior reflected a retuning of the control system for refuge tracking. We discovered that this retuning improved tracking performance, reduced sensitivity to disturbances, and improved PM. The effects of the retuning of the control system persisted after the destabilizing dynamics were removed, returning to baseline during a washout period. Interestingly, the time course of the return to baseline performance differed between the gain and phase of the sensorimotor transform.

This difference in the time course of return of gain and phase to baseline may be related to stability. To understand the effects of the different rates of return to baseline of gain (faster) and phase (slower) on closed-loop performance during the aftereffect period, it is helpful to consider the following counterfactual: what if the return to baseline did not occur? In other words, what if the controller that had been retuned in response to exposure to the augmented feedback at $k = 1.1$ did not return to baseline after the experiment? In this case, our calculations (not presented) indicate that the increased gain that resulted from retuning would have had substantial impacts on stability margins via a reduction in both the GMs and PMs during the aftereffect period compared with the baseline controller. In other words, the retuned controller was not well suited for the veridical condition.

This potentially destabilizing effect may be the reason for the relatively short timescale for the return of sensorimotor gain back to baseline. However, based on our calculations for this counterfactual exercise, the decreased phase lag that resulted from retuning would not have had a substantial impact on stability margins, creating less impetus for rapid de-adaptation of phase back to baseline. This finding is reminiscent of sensory reweighting in human postural control. Postural response gain decreases as stimulus switched to a higher amplitude, but phase of the response remained roughly constant.[42]

Neural substrates for retuning feedback control systems

The retuning of the controller for refuge tracking in *Eigenmannia* may be mediated, at least in part, by plasticity in cerebellum-like circuits.[43–46] Pairing of stimuli such as tail bending and electrosensory signals results in compensatory retuning of neurophysiological activity.[45] If pairing initially leads to an increase in firing, that firing may decrease as the pairing is repeated over periods of tens of seconds to minutes. Release of the pairing, in this example, results in a reduction in firing, known as a "negative image."[45] This negative image washes out over roughly the same time course as the initial retuning.

Such retuning has also been observed in cerebellar neurons that respond to moving objects.[43] These cerebellar neurons and other midbrain neurons exhibit direction-selective responses to moving objects.[45,47–52] Such direction-selective and other movement-sensitive neurons[53] may contribute to locomotor control used in the refuge tracking task and may be functionally linked to cerebellar retuning via the pretectum.[54]

Interestingly, experimental manipulation of the spectrum of background electrosensory noise results in a retuning of cerebellum-like[55] neurons in the electrosensory lateral line lobe (ELL), a hindbrain electrosensory nucleus in Gymnotiform fishes.[46] Specifically, the frequency tuning curves of neurons shift to maintain a "whitened" neurophysiological encoding across the behaviorally relevant spectrum.[56] These changes are mediated by a feedback pathway that also contributes to the perception of moving electrosensory stimuli.[57] Although speculative, the mechanisms underlying such retuning of the frequency responses of individual neurons may contribute to the frequency shift in the sensorimotor transform caused by the high-pass-filtered augmented feedback in this study.

In larval zebrafish (*Danio rerio*), several neural populations may contribute to the adaptation of motor systems to experimental manipulations of reafferent signals.[58–60] Zebrafish have an internal representation of the anticipated visual feedback for a given motor output—differences between the anticipated and actual feedback are error signals.[59] Zebrafish can use these error signals to adapt motor responses to changes in visual feedback. The activity of neurons recorded using two-photon calcium imaging in immobilized larval zebrafish suggests that retuning occurs in widespread neural populations, including populations in the inferior olive and cerebellum.[58] Lesions of the inferior olive reduced the ability of zebrafish to adapt their motor output to experimentally induced changes in feedback gain.[58]

The retuning of sensorimotor control circuits is also found in humans. Retuning can be seen, for example, in visuomotor tasks where participants reach toward a target.[10] Experimental rotations of visual feedback lead to a retuning of reaching dynamics. This retuning persists after the removal of the experimental manipulation,[10] which we also observed in *Eigenmannia*. A similar effect can be seen in experiments in which feedback during walking was manipulated using a split-belt treadmill.[61] In both of these examples, the time course of retuning is consistent with measures of cerebellar mechanisms. The effects of lesions

to cerebellar circuits in humans provides further evidence of the cerebellum's role in sensorimotor retuning, as such lesions result in impaired sensorimotor control adaptation.[62,63]

These neurophysiological and behavioral reports across species suggest that the sensorimotor retuning we observed in response to destabilizing reafferent dynamics are mediated, at least in part, by cerebellar or cerebellum-like circuits. Future neurophysiological and lesion studies of the ELL, cerebellum, and midbrain in *Eigenmannia* may reveal how retuning of sensorimotor gains in neural circuits leads to improvements in robustness.

Species differences in adaptation to altered feedback

In contrast to our findings in electric fish, fruit flies *Drosophila melanogaster* do not appear to adapt their optomotor response to changes in augmented feedback gain of wide-field stimuli.[29] A possible mechanism for this difference is that smooth pursuit object tracking (as in our study) and wide-field optic flow stabilization are mediated by fundamentally different learning and control mechanisms.[64–66] However, *Drosophila* may be able to adapt to gain reversals during object fixation.[28]

In humans and other vertebrates, visuomotor behavior readily adapts to a changing gain applied to wide-field optic flow stimuli, such as the gain adaptation and recalibration of the vestibulo-ocular reflex (VOR).[67–70] Moreover, it has been shown that modifying the gain between self-motion and optic flow cues induces plasticity in path integration.[71,72] Such wide-field gain adaptation, readily elicited in vertebrate species but not in *Drosophila*, may be related to adaptive control mechanisms in vertebrate nervous systems manifest in the cerebellum or cerebellum-like structures.[10]

Neural and mechanical contributions to robust performance

Robustness describes how well a system achieves stability and convergence despite external perturbations[17] or changes in internal parameters.[18] Retuning of control in response to novel dynamics is one mechanism to achieve such robust performance. We showed that *Eigenmannia* retune their control systems and, in so doing, increase PM and reduce sensitivity to low-frequency disturbances under augmented feedback. The maintenance of a robust PM, as we show here, is ecologically relevant because phase lag in sensory systems can depend greatly on environmental features, such as illumination[73] or conductivity,[22,74] which can affect sensorimotor delay.[73] Likewise, maintenance of robustness to mechanical disturbances enables hawkmoths to readily track moving flowers during feeding, despite experiencing perturbations in the form of vortices shed from flowers,[75] and humans to robustly reject mechanical disturbances during reaching.[76]

However, in closed-loop neuromechanical systems, robustness is not solely the purview of the nervous system. Indeed, failure to account for the dynamics of the musculoskeletal plant can lead to erroneous conclusions about neural control.[18,77,78] Stability and robust performance[18,20,79–82] result from the interplay between the mechanical and neural systems.[77] For example, mutually opposing forces produced by the ribbon fin of *Eigenmannia* enhance both stability and maneuverability, simplifying neural control.[27] Similarly, flies with damaged wings increase their damping coefficients to maintain stability during yaw gaze stabilization.[9] The flies achieve this through a decrease of closed-loop gain in the coupled system comprising body dynamics and neural control.

STAR★METHODS

Detailed methods are provided in the online version of this paper and include the following:

- KEY RESOURCES TABLE
- RESOURCE AVAILABILITY
  - Lead contact
  - Materials availability
  - Data and code availability
- EXPERIMENTAL MODEL AND SUBJECT DETAILS
  - Subjects
- METHOD DETAILS
  - Experimental apparatus
  - Innovations in augmented reafferent feedback
  - Experimental protocol
  - Online and offline tracking
  - System identification
  - Observed and simulated velocity tracking error
  - Normalized error and averaged frequency response error
  - Stability robustness analysis
  - Bode sensitivity integral
  - Model fitting
  - Setup delay analysis
- QUANTIFICATION AND STATISTICAL ANALYSIS

SUPPLEMENTAL INFORMATION

Supplemental information can be found online at https://doi.org/10.1016/j.cub.2024.04.019.

ACKNOWLEDGMENTS

We thank Balázs P. Vágvölgyi for modifying the experimental system; Lauren N. Peterson and Huanying Yeh for data collection and analysis; Sarah L. Poynton for critical feedback on the manuscript; and Christopher S. Yang, Debojyoti Biswas, and Di Cao for helpful discussions. We thank Kyle T. Yoshida, Ismail Uyanik, and Erin E. Sutton for pilot experiments. This work was supported by the Office of Naval Research under grant no. N00014-21-1-2431 (N.J.C) and the National Science Foundation under grant no. 2011619 (N.J.C).

AUTHOR CONTRIBUTIONS

Y.Y., D.G.Y., and N.J.C. co-designed the experiments; Y.Y. and D.G.Y. developed analysis methods; Y.Y. collected, processed, and analyzed data; N.J.C. oversaw data analysis, supervised the project, and obtained funding; Y.Y., E.S.F., and N.J.C. interpreted results; Y.Y. wrote the original draft; Y.Y., E.S.F., and N.J.C. co-edited the draft.

DECLARATION OF INTERESTS

The authors declare no competing interests.

Received: August 10, 2023
Revised: December 18, 2023
Accepted: April 9, 2024
Published: April 30, 2024

REFERENCES

1. Hughes, G.M. (1957). The co-ordination of insect movements: II. the effect of limb amputation and the cutting of commissures in the cockroach

(*Blatta orientalis*). J. Exp. Biol. *34*, 306–333. https://doi.org/10.1242/jeb.34.3.306.

2. Graham, D. (1977). The effect of amputation and leg restraint on the free walking coordination of the stick insect *Carausius morosus*. J. Comp. Physiol. *116*, 91–116. https://doi.org/10.1007/BF00605519.
3. Grabowska, M., Godlewska, E., Schmidt, J., and Daun-Gruhn, S. (2012). Quadrupedal gaits in hexapod animals–inter-leg coordination in free-walking adult stick insects. J. Exp. Biol. *215*, 4255–4266. https://doi.org/10.1242/jeb.073643.
4. Owaki, D., Aonuma, H., Sugimoto, Y., and Ishiguro, A. (2021). Leg amputation modifies coordinated activation of the middle leg muscles in the cricket *Gryllus bimaculatus*. Sci. Rep. *11*, 1327. https://doi.org/10.1038/s41598-020-79319-6.
5. Lockey, J.K., and Willis, M.A. (2015). One antenna, two antennae, big antennae, small: total antennae length, not bilateral symmetry, predicts odor-tracking performance in the american cockroach *Periplaneta americana*. J. Exp. Biol. *218*, 2156–2165. https://doi.org/10.1242/jeb.117721.
6. Dahake, A., Stöckl, A.L., Foster, J.J., Sane, S.P., and Kelber, A. (2018). The roles of vision and antennal mechanoreception in hawkmoth flight control. eLife *7*, e37606. https://doi.org/10.7554/eLife.37606.
7. Muijres, F.T., Iwasaki, N.A., Elzinga, M.J., Melis, J.M., and Dickinson, M.H. (2017). Flies compensate for unilateral wing damage through modular adjustments of wing and body kinematics. Interface Focus *7*, 20160103. https://doi.org/10.1098/rsfs.2016.0103.
8. Kihlström, K., Aiello, B., Warrant, E., Sponberg, S., and Stöckl, A. (2021). Wing damage affects flight kinematics but not flower tracking performance in hummingbird hawkmoths. J. Exp. Biol. *224*, jeb236240. https://doi.org/10.1242/jeb.236240.
9. Salem, W., Cellini, B., Kabutz, H., Hari Prasad, H.K., Cheng, B., Jayaram, K., and Mongeau, J.M. (2022). Flies trade off stability and performance via adaptive compensation to wing damage. Sci. Adv. *8*, eabo0719. https://doi.org/10.1126/sciadv.abo0719.
10. Krakauer, J.W., Hadjiosif, A.M., Xu, J., Wong, A.L., and Haith, A.M. (2019). Motor learning. Compr. Physiol. *9*, 613–663. https://doi.org/10.1002/cphy.c170043.
11. Bol, K., Marsat, G., Harvey-Girard, E., Longtin, A., and Maler, L. (2011). Frequency-tuned cerebellar channels and burst-induced LTD lead to the cancellation of redundant sensory inputs. J. Neurosci. *31*, 11028–11038. https://doi.org/10.1523/JNEUROSCI.0193-11.2011.
12. Dempsey, C., Abbott, L.F., and Sawtell, N.B. (2019). Generalization of learned responses in the mormyrid electrosensory lobe. eLife *8*, e44032. https://doi.org/10.7554/eLife.44032.
13. Mejias, J.F., Marsat, G., Bol, K., Maler, L., and Longtin, A. (2013). Learning contrast-invariant cancellation of redundant signals in neural systems. PLoS Comput. Biol. *9*, e1003180. https://doi.org/10.1371/journal.pcbi.1003180.
14. Gandolfo, F., Li, C.-S., Benda, B.J., Schioppa, C.P., and Bizzi, E. (2000). Cortical correlates of learning in monkeys adapting to a new dynamical environment. Proc. Natl. Acad. Sci. USA *97*, 2259–2263. https://doi.org/10.1073/pnas.040567097.
15. Dadarlat, M.C., Canfield, R.A., and Orsborn, A.L. (2023). Neural plasticity in sensorimotor brain–machine interfaces. Annu. Rev. Biomed. Eng. *25*, 51–76. https://doi.org/10.1146/annurev-bioeng-110220-110833.
16. Pratt, J.E., and Tedrake, R. (2006). Velocity-based stability margins for fast bipedal walking. In Fast Motions in Biomechanics and Robotics: Optimization and Feedback Control, M. Diehl, and K. Mombaur, eds. (Springer), pp. 299–324. https://doi.org/10.1007/978-3-540-36119-0_14.
17. Kitano, H. (2007). Towards a theory of biological robustness. Mol. Syst. Biol. *3*, 137. https://doi.org/10.1038/msb4100179.
18. Uyanik, I., Sefati, S., Stamper, S.A., Cho, K.A., Ankarali, M.M., Fortune, E.S., and Cowan, N.J. (2020). Variability in locomotor dynamics reveals the critical role of feedback in task control. eLife *9*, e51219. https://doi.org/10.7554/eLife.51219.
19. Cowan, N.J., Ankarali, M.M., Dyhr, J.P., Madhav, M.S., Roth, E., Sefati, S., Sponberg, S., Stamper, S.A., Fortune, E.S., and Daniel, T.L. (2014). Feedback control as a framework for understanding tradeoffs in biology. Integr. Comp. Biol. *54*, 223–237. https://doi.org/10.1093/icb/icu050.
20. Cowan, N.J., and Fortune, E.S. (2007). The critical role of locomotion mechanics in decoding sensory systems. J. Neurosci. *27*, 1123–1128. https://doi.org/10.1523/JNEUROSCI.4198-06.2007.
21. Biswas, D., Arend, L.A., Stamper, S.A., Vágvölgyi, B.P., Fortune, E.S., and Cowan, N.J. (2018). Closed-loop control of active sensing movements regulates sensory slip. Curr. Biol. *28*, 4029–4036.e4. https://doi.org/10.1016/j.cub.2018.11.002.
22. Stamper, S.A., Roth, E., Cowan, N.J., and Fortune, E.S. (2012). Active sensing via movement shapes spatiotemporal patterns of sensory feedback. J. Exp. Biol. *215*, 1567–1574. https://doi.org/10.1242/jeb.068007.
23. Chen, C., Murphey, T.D., and MacIver, M.A. (2020). Tuning movement for sensing in an uncertain world. eLife *9*, e52371. https://doi.org/10.7554/eLife.52371.
24. Biswas, D., Lamperski, A., Yang, Y., Hoffman, K., Guckenheimer, J., Fortune, E.S., and Cowan, N.J. (2023). Mode switching in organisms for solving explore-versus-exploit problems. Nat. Mach. Intell. *5*, 1285–1296. https://doi.org/10.1038/s42256-023-00745-y.
25. Rose, G.J., and Canfield, J.G. (1993). Longitudinal tracking responses of the weakly electric fish, *Sternopygus*. J. Comp. Physiol. A *171*, 791–798. https://doi.org/10.1007/BF00213075.
26. Roth, E., Zhuang, K., Stamper, S.A., Fortune, E.S., and Cowan, N.J. (2011). Stimulus predictability mediates a switch in locomotor smooth pursuit performance for *Eigenmannia virescens*. J. Exp. Biol. *214*, 1170–1180. https://doi.org/10.1242/jeb.048124.
27. Sefati, S., Neveln, I.D., Roth, E., Mitchell, T.R., Snyder, J.B., Maciver, M.A., Fortune, E.S., and Cowan, N.J. (2013). Mutually opposing forces during locomotion can eliminate the tradeoff between maneuverability and stability. Proc. Natl. Acad. Sci. USA *110*, 18798–18803. https://doi.org/10.1073/pnas.1309300110.
28. Wolf, R., Voss, A., Hein, S., and Heisenberg, M. (1992). Can a fly ride a bicycle? Phil. Trans. R. Soc. Lond. B *337*, 261–269. https://doi.org/10.1098/rstb.1992.0104.
29. Cellini, B., Ferrero, M., and Mongeau, J.M. (2024). *Drosophila* flying in augmented reality reveals the vision-based control autonomy of the optomotor response. Curr. Biol. *34*, 68–78.e4. https://doi.org/10.1016/j.cub.2023.11.045.
30. Yang, C.S., Cowan, N.J., and Haith, A.M. (2021). *De novo* learning versus adaptation of continuous control in a manual tracking task. eLife *10*, e62578. https://doi.org/10.7554/eLife.62578.
31. Sperry, R.W. (1943). Effect of 180 degree rotation of the retinal field on visuomotor coordination. J. Exp. Zool. *92*, 263–279. https://doi.org/10.1002/jez.1400920303.
32. Sperry, R.W. (1950). Neural basis of the spontaneous optokinetic response produced by visual inversion. J. Comp. Physiol. Psychol. *43*, 482–489. https://doi.org/10.1037/h0055479.
33. Kiemel, T., Zhang, Y., and Jeka, J.J. (2011). Identification of neural feedback for upright stance in humans: stabilization rather than sway minimization. J. Neurosci. *31*, 15144–15153. https://doi.org/10.1523/JNEUROSCI.1013-11.2011.
34. Yared, D.G. (2020). Learning of Novel Dynamics in *Eigenmannia virescens* Refuge Tracking Task. Master's thesis (Johns Hopkins University).
35. Finley, J.M., Long, A., Bastian, A.J., and Torres-Oviedo, G. (2015). Spatial and temporal control contribute to step length asymmetry during split-belt adaptation and hemiparetic gait. Neurorehabil. Neural Repair *29*, 786–795. https://doi.org/10.1177/1545968314567149.
36. Choi, J.T., and Bastian, A.J. (2007). Adaptation reveals independent control networks for human walking. Nat. Neurosci. *10*, 1055–1062. https://doi.org/10.1038/nn1930.

37. Roth, E., Sponberg, S., and Cowan, N.J. (2014). A comparative approach to closed-loop computation. Curr. Opin. Neurobiol. *25*, 54–62. https://doi.org/10.1016/j.conb.2013.11.005.

38. Åström, K.J., and Murray, R.M. (2021). Feedback Systems: An Introduction for Scientists and Engineers (Princeton University Press).

39. de C. Hamilton, A.F., Jones, K.E., and Wolpert, D.M. (2004). The scaling of motor noise with muscle strength and motor unit number in humans. Exp. Brain Res. *157*, 417–430. https://doi.org/10.1007/s00221-004-1856-7.

40. Combes, S.A., and Dudley, R. (2009). Turbulence-driven instabilities limit insect flight performance. Proc. Natl. Acad. Sci. USA *106*, 9105–9108. https://doi.org/10.1073/pnas.0902186106.

41. Csete, M.E., and Doyle, J.C. (2002). Reverse engineering of biological complexity. Science *295*, 1664–1669. https://doi.org/10.1126/science.1069981.

42. Carver, S., Kiemel, T., and Jeka, J.J. (2006). Modeling the dynamics of sensory reweighting. Biol. Cybern. *95*, 123–134. https://doi.org/10.1007/s00422-006-0069-5.

43. Bastian, J. (1975). Receptive fields of cerebellar cells receiving exteroceptive input in a gymnotid fish. J. Neurophysiol. *38*, 285–300. https://doi.org/10.1152/jn.1975.38.2.285.

44. Bell, C., Bodznick, D., Montgomery, J., and Bastian, J. (1997). The generation and subtraction of sensory expectations within cerebellum-like structures. Brain Behav. Evol. *50* (*Supplement 1*), 17–31. https://doi.org/10.1159/000113352.

45. Bastian, J. (1996). Plasticity in an electrosensory system. I. General features of a dynamic sensory filter. J. Neurophysiol. *76*, 2483–2496. https://doi.org/10.1152/jn.1996.76.4.2483.

46. Huang, C.G., Metzen, M.G., and Chacron, M.J. (2019). Descending pathways mediate adaptive optimized coding of natural stimuli in weakly electric fish. Sci. Adv. *5*, eaax2211. https://doi.org/10.1126/sciadv.aax2211.

47. Bastian, J. (1982). Vision and electroreception: integration of sensory information in the optic tectum of the weakly electric fish *Apteronotus albifrons*. J. Comp. Physiol. *147*, 287–297. https://doi.org/10.1007/BF00609662.

48. Ramcharitar, J.U., Tan, E.W., and Fortune, E.S. (2006). Global electrosensory oscillations enhance directional responses of midbrain neurons in *Eigenmannia*. J. Neurophysiol. *96*, 2319–2326. https://doi.org/10.1152/jn.00311.2006.

49. Fortune, E.S. (2006). The decoding of electrosensory systems. Curr. Opin. Neurobiol. *16*, 474–480. https://doi.org/10.1016/j.conb.2006.06.006.

50. Chacron, M.J., Toporikova, N., and Fortune, E.S. (2009). Differences in the time course of short-term depression across receptive fields are correlated with directional selectivity in electrosensory neurons. J. Neurophysiol. *102*, 3270–3279. https://doi.org/10.1152/jn.00645.2009.

51. Chacron, M.J., and Fortune, E.S. (2010). Subthreshold membrane conductances enhance directional selectivity in vertebrate sensory neurons. J. Neurophysiol. *104*, 449–462. https://doi.org/10.1152/jn.01113.2009.

52. Khosravi-Hashemi, N., Fortune, E.S., and Chacron, M.J. (2011). Coding movement direction by burst firing in electrosensory neurons. J. Neurophysiol. *106*, 1954–1968. https://doi.org/10.1152/jn.00116.2011.

53. Clarke, S.E., Naud, R., Longtin, A., and Maler, L. (2013). Speed-invariant encoding of looming object distance requires power law spike rate adaptation. Proc. Natl. Acad. Sci. USA *110*, 13624–13629. https://doi.org/10.1073/pnas.1306428110.

54. Keller, C.H., Maler, L., and Heiligenberg, W. (1990). Structural and functional organization of a diencephalic sensory-motor interface in the gymnotiform fish, *Eigenmannia*. J. Comp. Neurol. *293*, 347–376. https://doi.org/10.1002/cne.902930304.

55. Bell, C.C. (2002). Evolution of cerebellum-like structures. Brain Behav. Evol. *59*, 312–326. https://doi.org/10.1159/000063567.

56. Huang, C.G., Metzen, M.G., and Chacron, M.J. (2018). Feedback optimizes neural coding and perception of natural stimuli. eLife *7*, e38935. https://doi.org/10.7554/eLife.38935.

57. Clarke, S.E., and Maler, L. (2017). Feedback synthesizes neural codes for motion. Curr. Biol. *27*, 1356–1361. https://doi.org/10.1016/j.cub.2017.03.068.

58. Ahrens, M.B., Li, J.M., Orger, M.B., Robson, D.N., Schier, A.F., Engert, F., and Portugues, R. (2012). Brain-wide neuronal dynamics during motor adaptation in zebrafish. Nature *485*, 471–477. https://doi.org/10.1038/nature11057.

59. Portugues, R., and Engert, F. (2011). Adaptive locomotor behavior in larval zebrafish. Front. Syst. Neurosci. *5*, 72. https://doi.org/10.3389/fnsys.2011.00072.

60. Engert, F. (2012). Fish in the matrix: motor learning in a virtual world. Front. Neural Circuits *6*, 125. https://doi.org/10.3389/fncir.2012.00125.

61. Reisman, D.S., Block, H.J., and Bastian, A.J. (2005). Interlimb coordination during locomotion: what can be adapted and stored? J. Neurophysiol. *94*, 2403–2415. https://doi.org/10.1152/jn.00089.2005.

62. Martin, T.A., Keating, J.G., Goodkin, H.P., Bastian, A.J., and Thach, W.T. (1996). Throwing while looking through prisms: I. Focal olivocerebellar lesions impair adaptation. Brain *119*, 1183–1198. https://doi.org/10.1093/brain/119.4.1183.

63. Therrien, A.S., and Bastian, A.J. (2015). Cerebellar damage impairs internal predictions for sensory and motor function. Curr. Opin. Neurobiol. *33*, 127–133. https://doi.org/10.1016/j.conb.2015.03.013.

64. Hardcastle, B.J., and Krapp, H.G. (2016). Evolution of biological image stabilization. Curr. Biol. *26*, R1010–R1021. https://doi.org/10.1016/j.cub.2016.08.059.

65. Mongeau, J.M., and Frye, M.A. (2017). *Drosophila* spatiotemporally integrates visual signals to control saccades. Curr. Biol. *27*, 2901–2914.e2. https://doi.org/10.1016/j.cub.2017.08.035.

66. Frighetto, G., and Frye, M.A. (2023). Columnar neurons support saccadic bar tracking in *Drosophila*. eLife *12*, e83656. https://doi.org/10.7554/eLife.83656.

67. Shelhamer, M., Tiliket, C., Roberts, D., Kramer, P.D., and Zee, D.S. (1994). Short-term vestibulo-ocular reflex adaptation in humans: II. Error signals. Exp. Brain Res. *100*, 328–336. https://doi.org/10.1007/BF00227202.

68. Kramer, P., Shelhamer, M., and Zee, D.S. (1998). Short-term vestibulo-ocular adaptation: influence of context. Otolaryngol. Head Neck Surg. *119*, 60–64. https://doi.org/10.1016/S0194-5998(98)70174-3.

69. Nagao, S. (1983). Effects of vestibulocerebellar lesions upon dynamic characteristics and adaptation of vestibulo-ocular and optokinetic responses in pigmented rabbits. Exp. Brain Res. *53*, 36–46. https://doi.org/10.1007/BF00239396.

70. Iwashita, M., Kanai, R., Funabiki, K., Matsuda, K., and Hirano, T. (2001). Dynamic properties, interactions and adaptive modifications of vestibulo-ocular reflex and optokinetic response in mice. Neurosci. Res. *39*, 299–311. https://doi.org/10.1016/s0168-0102(00)00228-5.

71. Rieser, J.J., Pick, H.L., Ashmead, D.H., and Garing, A.E. (1995). Calibration of human locomotion and models of perceptual-motor organization. J. Exp. Psychol. Hum. Percept. Perform. *21*, 480–497. https://doi.org/10.1037//0096-1523.21.3.480.

72. Madhav, M.S., Jayakumar, R.P., Li, B., Savelli, F., Knierim, J.J., and Cowan, N.J. (2022). Closed-loop control and recalibration of place cells by optic flow. Preprint at BioRxiv. https://doi.org/10.1101/2022.06.12.495823.

73. Sponberg, S., Dyhr, J.P., Hall, R.W., and Daniel, T.L. (2015). Luminance-dependent visual processing enables moth flight in low light. Science *348*, 1245–1248. https://doi.org/10.1126/science.aaa3042.

74. MacIver, M.A., Sharabash, N.M., and Nelson, M.E. (2001). Prey-capture behavior in gymnotid electric fish: motion analysis and effects of water conductivity. J. Exp. Biol. *204*, 543–557. https://doi.org/10.1242/jeb.204.3.543.

75. Matthews, M., and Sponberg, S. (2018). Hawkmoth flight in the unsteady wakes of flowers. J. Exp. Biol. *221*, jeb179259. https://doi.org/10.1242/jeb.179259.

76. Crevecoeur, F., Scott, S.H., and Cluff, T. (2019). Robust control in human reaching movements: a model-free strategy to compensate for

unpredictable disturbances. J. Neurosci. *39*, 8135–8148. https://doi.org/10.1523/JNEUROSCI.0770-19.2019.

77. Full, R.J., Kubow, T., Schmitt, J., Holmes, P., and Koditschek, D. (2002). Quantifying dynamic stability and maneuverability in legged locomotion. Integr. Comp. Biol. *42*, 149–157. https://doi.org/10.1093/icb/42.1.149.
78. Dickinson, M.H., Farley, C.T., Full, R.J., Koehl, M.A., Kram, R., and Lehman, S. (2000). How animals move: an integrative view. Science *288*, 100–106. https://doi.org/10.1126/science.288.5463.100.
79. Tytell, E.D., Holmes, P., and Cohen, A.H. (2011). Spikes alone do not behavior make: why neuroscience needs biomechanics. Curr. Opin. Neurobiol. *21*, 816–822. https://doi.org/10.1016/j.conb.2011.05.017.
80. Miller, L.A., Goldman, D.I., Hedrick, T.L., Tytell, E.D., Wang, Z.J., Yen, J., and Alben, S. (2012). Using computational and mechanical models to study animal locomotion. Integr. Comp. Biol. *52*, 553–575. https://doi.org/10.1093/icb/ics115.
81. Madhav, M.S., and Cowan, N.J. (2020). The synergy between neuroscience and control theory: the nervous system as inspiration for hard control challenges. Annu. Rev. Control Robot. Auton. Syst. *3*, 243–267. https://doi.org/10.1146/annurev-control-060117-104856.
82. Carryon, G.N., and Tangorra, J.L. (2020). The effect of sensory feedback topology on the entrainment of a neural oscillator with a compliant foil for swimming systems. Bioinspir. Biomim. *15*, 046013. https://doi.org/10.1088/1748-3190/ab76a0.
83. Hitschfeld, E.M., Stamper, S.A., Vonderschen, K., Fortune, E.S., and Chacron, M.J. (2009). Effects of restraint and immobilization on electrosensory behaviors of weakly electric fish. ILAR J. *50*, 361–372. https://doi.org/10.1093/ilar.50.4.361.
84. Mathis, A., Mamidanna, P., Cury, K.M., Abe, T., Murthy, V.N., Mathis, M.W., and Bethge, M. (2018). DeepLabCut: Markerless pose estimation of user-defined body parts with deep learning. Nat. Neurosci. *21*, 1281–1289. https://doi.org/10.1038/s41593-018-0209-y.
85. Yang, Y. (2020). A Comparison of System Identification Techniques for Refuge Tracking Behavior in *Eigenmannia virescens*. Master's thesis (Johns Hopkins University).
86. Zimmet, A.M., Cao, D., Bastian, A.J., and Cowan, N.J. (2020). Cerebellar patients have intact feedback control that can be leveraged to improve reaching. eLife *9*, e53246. https://doi.org/10.7554/eLife.53246.
87. Cardillo, G. (2018). MWWTEST: Mann-whitney-wilcoxon non parametric test for two unpaired samples. http://www.mathworks.com/matlabcentral/fileexchange/25830.

STAR★METHODS

KEY RESOURCES TABLE

REAGENT or RESOURCE	SOURCE	IDENTIFIER
Deposited Data		
Behavioral (fish refuge tracking) data	This paper	Johns Hopkins Research Data Repository: https://doi.org/10.7281/T1/F5PD42
Software and algorithms		
MATLAB R2022b	The MathWorks Inc., Natick, MA	RRID: SCR_001622 https://www.mathworks.com/
LabVIEW	National Instruments 2015, Service Pack[1]	RRID: SCR_014325 http://www.ni.com/labview/
Affinity Designer 1.10.5.1342	Serif (Europe) Ltd	RRID: SCR_016952 https://affinity.serif.com/en-us/
Code and algorithms	This paper	Johns Hopkins Research Data Repository: https://doi.org/10.7281/T1/F5PD42
Experimental models: Organisms/strains		
Eigenmannia virescens	Segrest Farms, Gibsonton, Florida	Noah J. Cowan, Johns Hopkins University

RESOURCE AVAILABILITY

Lead contact

Further information and requests for data/protocols should be directed to and will be fulfilled by the lead contact, Noah J. Cowan (ncowan@jhu.edu).

Materials availability

This study did not generate new unique reagents.

Data and code availability

The archived version of the datasets and the analysis code supporting this article are available through the Johns Hopkins University Data Repository with the following DOI: https://doi.org/10.7281/T1/F5PD42.

EXPERIMENTAL MODEL AND SUBJECT DETAILS

Subjects

Adult weakly electric glass knifefish *Eigenmannia virescens* (length: 10–15 cm) were obtained from commercial vendors and housed following published guidelines.[83] Temperature and conductivity of the water in the experimental aquarium were kept at 76° F–80° F and 10 μS/cm–150 μS/cm, respectively. All fish were transferred to the experimental aquarium 12–24 hours before the start of the experiments. The experiments were conducted under an illuminance level of approximately 80 lux. Experimental procedures were approved by the Johns Hopkins Animal Care and Use Committee and followed guidelines established by the National Research Council and the Society for Neuroscience.

METHOD DETAILS

Experimental apparatus

The experimental apparatus was similar to that used by Biswas et al.[21] This system measured the position of the fish within a moving refuge in real-time. The measurement of fish position was available for the control of the movement of the refuge, allowing adjustment of refuge movement in relation to fish behavior. The movement of the shuttle was determined by two signals: (i) a high-pass filtered measurement of the velocity of the fish, and (ii) a static sum-of-sines velocity signal.[34] We refer to this high-pass-filtered feedback as "augmented reafferent feedback."

Innovations in augmented reafferent feedback

To facilitate the experimental investigation of the learning process, we used a high-pass filter for the augmented feedback. The high-pass filtered feedback, unlike a simple static gain, enables the graceful, parametric destabilization of the closed-loop system. To understand this distinction, consider the $k = 1.0$ case. For static feedback (i.e., a pure gain with no high-pass filter), $k = 1.0$ cancels the

veridical reafferent feedback leading to a singularity: the refuge would track the fish in 1-to-1 fashion, making it impossible for the fish to volitionally swim to a desired location within the refuge and therefore making it physically impossible for *any* retuning of the controller to stabilize the system.

In this augmented environment, a static gain of $k > 1$ is analogous to a mirror reversal in virtual visuomotor tasks, since, as the fish swims forward relative to the tank, the refuge moves forward *even more*, so that the sign of the error signal is reversed (i.e. the fish ends up further back within the refuge, even though it swam forward in this hypothetical scenario). Thus, experimentally transitioning from stable augmented feedback $k < 1$ to destabilizing mirror reversal $k > 1$ would require discretely jumping over the inescapable singularity at $k = 1$, thereby introducing dramatic and abrupt changes in stability.

The key innovation of the high-pass filter approach is that *it does not alter the low-frequency dynamics* (i.e., below the filter cut-off frequency), yet still can reverse the sign of the high-frequency feedback (i.e., above the filter cut-off frequency), destabilizing the system as the gain increases—but with no singularity. This is seen in our experiments in which we gracefully transition to high-frequency mirror reversal, incrementally increasing the gain from $k = 0$ to $k = 1.1$, gradually reversing the sign of high-frequency error feedback while leaving low-frequency feedback unchanged.

Experimental protocol

Our intention was to drive the entire closed-loop system toward instability by increasing the gain of the augmented feedback. We examined the sensorimotor transform that fish used to maintain their position with the refuge before (“baseline”), during the augmented feedback period of increasing gain (“closed-loop”), and after the augmented feedback period (“aftereffect”). Both “baseline” and “aftereffect” periods were open-loop (no high-pass-filter feedback); the “closed-loop” period had the high-pass-filter feedback.

During the baseline period, we conducted five 60 sec stimulus–response trials, with a 20 sec “rest” period between each trial. The input stimulus during each trial comprised a 10 sec ramp-up, 40 sec of sum-of-sines inputs, and 10 sec ramp-down (see Figure S1A), described in detail below in relation to Equation 2. Rest periods had zero movement instead of the sum-of-sines stimulus ($r(t) = 0$).

In the closed-loop period, there was a first order high-pass filter in the augmented feedback loop. The high-pass filter gain k was increased incrementally: from 0.3, 0.6, 0.8, and 1.0, to 1.1 (Figure 1C). The upper limit of $k = 1.1$ was chosen based on preliminary analysis[34] that indicated gains above approximately 1.3 would completely destabilize the baseline controller. Preliminary attempts to approach this gain led to frequent transient movements of the refuge that hit travel limits of the apparatus.[34] For this reason, we set the upper limit to $k = 1.1$ as a balance between driving the system toward instability while respecting the practical constraints of the experimental apparatus.

In each feedback period ($k = 0.3, 0.6, 0.8, 1.0, 1.1$), there were five trials (60 sec each) with four rest periods (20 sec each, $r(t) = 0$) in between. Critically, the augmented feedback remained enabled during these rest periods. There were also 20 sec rest periods connecting the last trial of each feedback period to the first trial in the next feedback period. During these inter-trial rest periods, the feedback gain was linearly increased as a function of time from the last value of k to the next value (so that the gain changed gradually, rather than abruptly). During all rest periods, no pre-defined reference inputs were used, i.e., $r(t) = 0$.

At the start of the aftereffect period, the augmented feedback was abruptly extinguished ($k = 0$). Aftereffects were measured during five non-overlapping time intervals after the closed-loop augmented feedback was extinguished: “0 to 5 min,” “5 to 10 min,” “10 to 15 min,” “15 to 21 min,” and “next day.” The input stimulus and the duration of rest periods were the same as those in baseline period. Three trials were conducted for each subsequent 5 min period and five trials were conducted for the 15 to 21 min and next day after periods.

The pre-designed reference stimulus signal had three periods: “ramp-up,” “sum-of-sines,” and “ramp-down,” as illustrated in Figure S1A. In ramp-up and ramp-down periods, the designed signal oscillated at 0.45 Hz with modulated amplitude, and was added to the modulated sum-of-sines signal (Figure S1A). The sum of 12 single sinusoidal functions, $r_1(t)$, is given (in centimeters) as follows:

$$r_1(t) = 0.8 \sum_{i=1}^{12} \frac{1}{2\pi 0.05 k_i} \cdot \cos(2\pi 0.05 k_i t + \Phi_i). \quad \text{(Equation 2)}$$

Here, $k_i = 2, 3, 5, 7, 11, 13, 19, 23, 29, 31, 37, 41$ are prime numbers and the phase of each single sine component Φ_i is randomized. This function creates a pseudo-random, unpredictable stimulus, suitable for system identification.[26]

Online and offline tracking

The refuge position and fish position were both measured in real time by a template matching tracker in LabVIEW,[21] with a sampling rate of 25 frames per sec. We also performed offline tracking of fish and refuge motion using the tracking software DeepLabCut.[84]

System identification

After obtaining the refuge and fish position in the time domain, we performed system identification with seven fish. The system identification procedure was similar to Yang.[85] For each of the three experimental periods (baseline, closed-loop, and aftereffect), we processed the middle 40 sec sum-of-sines part of each trial and divided it into two halves to double the replicates of data (since the stimulus was designed to repeat every 20 sec). We then took the mean of each batch of 20 sec input and output position data in each period (baseline, five feedback periods in closed-loop period, and five time intervals in aftereffect period) and

transformed the mean positon data into the frequency domain using discrete Fourier transform (DFT). We then used an empirical transfer function estimate (ETFE) to estimate the Frequency Response Function (FRF) for each period.

Note that for two fish (fish 1 and 4), due to data quality of baseline trials and the similarity of trials in baseline and next day after, we combined the time domain data in these periods to estimate the baseline FRF. Trials with tracking loss were discarded. Data from two fish (fish 2 and 3) were excluded for $k = 1.1$ due to tracking loss by the control system during the experiment.

Observed and simulated velocity tracking error

The velocity tracking error $\dot{e}(t)$ is defined as the difference of refuge velocity $\dot{s}(t)$ and fish velocity $\dot{y}(t)$, i.e., $\dot{e}(t) = \dot{s}(t) - \dot{y}(t)$. The refuge and fish velocities were computed using the backward difference of the position time series data and filtered through a second-order Butterworth zero-phase distortion filter using the MATLAB *filtfilt* command with 5 Hz cutoff. To examine how the retuned controllers affected fish tracking performance, we simulated the velocity tracking error in each augmented feedback period using each fish's baseline controller under the assumption that fish did not retune their controllers under augmented feedback, and compared the simulated velocity tracking error with experimental data.

We followed the following steps to simulate the velocity tracking error in each augmented feedback period.

Step 1

We computed the FRFs from the reference sum-of-sines signal $r(t)$ to the sensory slip $e(t)$ in each augmented feedback period from control theory:

$$\frac{E(j\omega)}{R(j\omega)} = \frac{D(j\omega)}{1+C(j\omega)P(j\omega) - C(j\omega)P(j\omega)D(j\omega)H(j\omega)}, \quad \text{(Equation 3)}$$

where $j = \sqrt{-1}$, ω is the frequency in rad/sec,

$$H(j\omega) = \frac{kj\omega}{j\omega+1} \quad \text{(Equation 4)}$$

is a first order high-pass filter in augmented reafferent feedback, $D(j\omega)$ is a delay caused by experimental apparatus latencies (Figure S4), and $C(j\omega)$ and $P(j\omega)$ are the FRF of the fish controller and plant, respectively (Figures 1B and S4). All terms on right hand side of Equation 3 were either known or could be estimated: we knew the designed augmented reafferent feedback $H(j\omega)$; we estimated $D(j\omega)$ from online to offline refuge position via ETFE; the multiplication of FRF of $C(j\omega)$ and $P(j\omega)$ was computed from the estimated fish's FRFs by opening the fish's veridical reafferent feedback loop.

Step 2

We reconstructed the simulated sensory slip $e_{\text{sim}}(t)$ by following equation:

$$e_{\text{sim}}(t) = 0.8\sum_{i=1}^{12}\left|\frac{E(j\omega_i)}{R(j\omega_i)}\right| \cdot \frac{1}{\omega_i} \cdot \cos\left(\omega_i t + \Phi_i + \angle\frac{E(j\omega_i)}{R(j\omega_i)}\right). \quad \text{(Equation 5)}$$

where, $\omega_i = 2\pi \times 0.05 \times [2,3,5,7,11,13,19,23,29,31,37,41]$, Φ_i is the randomized phase of each single sine component in the reference signal $r(t)$, $|E(j\omega_i)/R(j\omega_i)|$ and $\angle E(j\omega_i)/R(j\omega_i)$ are the amplitude and phase of the complex number $E(j\omega_i)/R(j\omega_i)$.

Step 3

Finally, to mimic the way we processed position real data to obtain velocity data, we computed the simulated velocity tracking error $\dot{e}_{\text{sim}}(t)$ using backward differences of $e_{\text{sim}}(t)$, filtered through a second-order Butterworth zero-phase distortion filter using MATLAB *filtfilt* command with 5 Hz cutoff frequency.

Normalized error and averaged frequency response error

To evaluate fish tracking performance, the normalized frequency domain error was computed in each augmented feedback period by taking the magnitude of the ratio of the mean sensory slip $E(j\omega)$ to reference signal $R(j\omega)$ (at frequency components contained by the reference signal). The frequency domain sensory slip $E(j\omega)$ and the reference signal $R(j\omega)$ were computed using the DFT. The sensory slip was calculated (in the time domain) as $e(t) = s(t) - y(t)$.

From each fish's baseline controller, we predicted the normalized error that would have occurred during a feedback period (assuming the fish had not retuned its controller), and compared that predicted error with the normalized error measured from experimental data (where the fish had ample opportunity to retune its controller). To quantify the impacts of the retuned controller on tracking error across the frequency range $0.1 - 2.05$ Hz, we estimated the integral of the normalized error using trapezoidal integration, and divided this integral by the frequency range to obtain the averaged frequency response error. Note that although in Figure 4C the x and y axes are both shown using a logarithmic scale, we computed the intergal of the normalized error using a linear scale.

Stability robustness analysis

The two margins of stability, gain margin (GM) and phase margin (PM), reflect the stability robustness of the closed-loop system. When the margins of stability decrease, the system becomes less robust. To compute stability margin, one must compute the loop function

$$L(s) = C(s)P(s) - C(s)P(s)D(s)H(s), \quad \text{(Equation 6)}$$

where $s = j\omega, j = \sqrt{-1}$, $H(s)$ is the first order high-pass filter in augmented reafferent feedback, and $D(s)$ is the setup delay in the forward loop. The multiplication of transfer function of controller, i.e., $C(s)$, and that of plant, i.e., $P(s)$, could be computed from the estimated fish's FRFs by opening the fish's reafferent feedback loop. The transfer function in the augmented feedback was known, so the loop function was then computed, and another array of complex numbers was obtained.

The system becomes unstable if $L(j\omega) = -1$ (i.e., 0 dB with phase -180°). So, the GM was computed as 0 minus the gain (in dB) at the phase cross-over frequency (the frequency at which the phase of $L(j\omega)$ crosses -180°). Likewise, the PM was calculated by computing the phase at the gain cross-over frequency (the frequency at which $|L(j\omega)|$ crosses 0 dB), and subtracting -180°. These computations make certain technical assumptions on L that are satisfied by a wide range of systems. For example, we must assume that the Nyquist stability criterion for L requires that $L(j\omega)$ must have no encirclements of the -1 point on the complex plane, an assumption that is consistent with our fitted models.

A key question was to determine how the modified controller during closed-loop experiments impacted the stability robustness of the closed-loop system. To address this, we compared the observed GMs and PMs from the fish loop function at each feedback period with predicted GMs and PMs.

Bode sensitivity integral

The sensitivity function is defined as follows:

$$S(s) = \frac{1}{1+L(s)}, \quad \text{(Equation 7)}$$

where $s = j\omega, j = \sqrt{-1}$ and $L(s)$ is the loop function defined above. Thus, we could directly compute the sensitivity function from the loop function. Plugging in (Equation 6) to (Equation 7) yields $S = 1/(1 + CP - CPDH)$.

To calculate the Bode sensitivity integral over the frequency range $0.2\pi - 4.1\pi$ rad/sec, we used trapezoidal integration of Equation 1 (Figure 5A).

The Bode integral condition in Equation 1 assumes that the loop function L satisfies two conditions: 1) has no unstable poles (a pole at $s = 0$ is allowed), and 2) has at least two more poles than zeros. The electric fish plant dynamics $P(s)$ have been modeled using physics[27] and system identification[18] as a relative-degree 2, second-order transfer function with no zeros, a pole at 0, and a pole in the open left-half-plane. Assuming the fish controller $C(s)$ is causal and stable, and thus is proper, then one can show that the loop function $L = CP - CPDH$ satisfies the two conditions above for the Bode sensitivity integral to be 0.

Model fitting

The calculation of PM and GM is the only analysis in the paper that involved model fitting. This is because the exact gain and phase cross-over frequencies must be interpolated or extrapolated from the data, and we used fitted models. We fitted the fish controller and plant cascade, $C(s)P(s)$, with a second order model (relative degree one: 2 poles, 1 zero with delay):

$$C(s)P(s)_{\text{model1}} = \frac{k_1 s + k_2}{s^2 + k_3 s + k_4} e^{-\tau_d s}, \quad \text{(Equation 8)}$$

and a third order model (relative degree two: three poles, 1 zero with delay)

$$C(s)P(s)_{\text{model2}} = \frac{k_1 s + k_2}{s^3 + k_3 s^2 + k_4 s + k_5} e^{-\tau_d s}. \quad \text{(Equation 9)}$$

Note that parameters of these two models were fitted independently. Both models fitted the $C(s)P(s)$ data well. The third order model fitted the data slightly better than the second order model as expected (because the former contained one additional parameter); however, the third order model was prone to overfitting. Therefore, for the purpose of analysis, we used the simpler second order model in Equation 8.

To select the best fit model, we followed three steps.

Step 1: Define the fitting error

The frequency response of each feedback period was represented as a vector of 12 complex numbers:

$$G_{\text{raw}} = [m_1 + jn_1, m_2 + jn_2, \ldots, m_{12} + jn_{12}], \quad \text{(Equation 10)}$$

one for each frequencies that was contained in the reference sum-of-sines stimulus,[26,86] where $j = \sqrt{-1}$.

Similarly, we obtained frequency response functions at these 12 frequencies directly from the fitted model with $s = j\omega$, noted as:

$$G_{\text{modeled}} = [p_1 + jq_1, p_2 + jq_2, \cdots, p_{12} + jq_{12}]. \quad \text{(Equation 11)}$$

The fitting error is defined as the mean-squared error between G_{raw} and G_{modeled}, i.e.,

$$\text{Fitting Error} = \frac{1}{12}\|G_{\text{raw}} - G_{\text{modeled}}\|^2, \quad \text{(Equation 12)}$$

where $\|\cdot\|$ is the 2-norm of vector.

Step 2: Use MATLAB function to obtain sets of optimal parameters in candidate model that minimize the fitting error corresponding to different initial conditions

As an example, the second order model (relative degree one: 2 poles, 1 zero with delay) has five parameters: k_1, k_2, k_3, k_4, and τ_d. We randomly generated 500 sets of initial values for each of those five parameters. Then we used MATLAB function *fminsearch* to find 500 sets of optimal parameters [k_1, k_2, k_3, k_4, τ_d] that made the fitting error reach the local minimum from each initial condition.

Step 3: Select the least fitting error among sets of optimal parameters

Finally, we selected a set of parameters, among all 500 sets of optimal parameters corresponding to each initial condition, that gave the least fitting error.

Setup delay analysis

The latencies in the experimental setup can impact the accuracy of estimated fish's FRF in system identification, and this needs to be taken into consideration when analyzing our data. In our system, the delay was mainly the latencies between reading the reference files from the PC and trigger of the linear actuator to control the refuge movement. There were only negligible delays caused by other factors such as asynchronously saving the videos and tracking files, and the augmented feedback processing delay from FPGA.

Delay is modeled by the transfer function $e^{-\tau s}$, where τ is the delay. Here we denote the system delay as $D(s)$ (Figure S4). To generate the offline refuge movement data, we processed recorded experimental videos with the tracking software DeepLabCut,[84] and estimated the delay in the frequency domain by taking the ratio of the Fourier domain offline refuge trajectories, to the Fourier domain online refuge trajectories saved from the experimental setup.

QUANTIFICATION AND STATISTICAL ANALYSIS

All the statistical analysis was performed in MATLAB (Mathworks, Natick, Massachusetts, USA). Specifically, we used function *corrcoef* to test correlation coefficients of data points. We used function *ttest* to perform paired-sample *t* test, used function *signtest* to perform two-sided sign test, and used function *mwwtest*[87] for the two tailed Mann-Whitney-Wilcoxon (MWW) test. For all tests, the significance level was 0.05.